Quaternary Science Reviews 308 (2023) 108041

Contents lists available at ScienceDirect

Quaternary Science Reviews

journal homepage: www.elsevier.com/locate/quascirev

# Reconstructing terrestrial ice sheet retreat dynamics from hummocky topography using multiscale evidence: An example from central Ireland

Catherine A. Delaney [a, *], Kathryn Adamson [a], Lorna D. Linch [b], Stephen Davis [c], Stephen McCarron [d]

[a] School of Science and the Environment, Manchester Metropolitan University, John Dalton East, Chester St., Manchester, M1 5GD, UK
[b] School of Applied Sciences, University of Brighton, Cockcroft Building, Lewes Road, Brighton, BN2 4GJ, UK
[c] School of Archaeology, University College, Dublin, Ireland
[d] Department of Geography, Maynooth University, Ireland

ARTICLE INFO

*Article history:*
Received 10 October 2022
Received in revised form
9 March 2023
Accepted 10 March 2023
Available online xxx

Handling Editor: C. Hillaire-Marcel

*Keywords:*
Pleistocene
Glaciology
Western Europe
Glacial geomorphology
Hummocky topography
Ribbed moraine
LiDAR
Ground-penetrating radar
Micromorphology
Ireland

ABSTRACT

The research reported here combines high-resolution digital elevation models (DEMs) derived from airborne LiDAR with ground-penetrating radar (GPR) surveys and macro- and micro-scale sedimentological analyses to study the geomorphology and internal structure and composition of ridges and mounds within an area of hummocky topography in the Brosna basin, central Ireland. Our evidence indicates that much of the hummocky topography consists of fragmented mega-scale glacial lineations (MSGLs) indicating a phase of accelerated ice flow, overlain by groups of small ridges composed of subglacially derived till and sediment gravity flow deposits. Subtle differences in ridge morphology indicate they may be multi-genetic and formed both ice-marginally as moraines and subglacially as small ribbed moraine. We interpret MSGL-ridge associations as a subglacial bedform continuum reflecting the evolution from a deforming bed to brittle deformation, due to changing thermal and hydrological conditions at the ice-bed interface during ice sheet retreat. Adjacent glaciofluvial landforms indicate initial en- and supra-glacial meltwater drainage, possibly directly related to changing basal thermal/hydrological characteristics and subglacial ridge formation. Subsequently a subglacial conduit system evolved, and later retreat involved formation of ice-marginal ridges. The partially preserved landsystem reflects formation at a polythermal to active temperate ice marginal zone, rather than the stagnating temperate margin previously assumed for this area. Our work demonstrates the usefulness of hummocky topography in identifying changes in ice sheet bed thermal/hydrological characteristics during deglaciation and the importance of combining multiple evidence strands in reconstructing the processes involved in glacial landform construction.



## 1. Introduction

The beds of modern ice sheets are mostly inaccessible. Therefore, the record of glacial landforms left behind by former ice sheets is crucial to understanding and predicting the dynamics of contemporary ice sheets (e.g. Kleman and Applegate, 2014). Large, laterally continuous landforms including subglacial bedforms (e.g. drumlins, mega-scale glacial lineations (MSGLs), crag-and-tails, ribs, streamlined bedrock), meltwater landforms (e.g. meltwater channels, eskers, glaciofluvial deposits, ice-contact deltas) and moraines have been used to reconstruct the retreat characteristics of all major Quaternary ice sheets (e.g. Dyke and Prest, 1987; Dyke et al., 2002; Hughes et al., 2016; Clark et al., 2012; Clark et al., 2018; Boyes et al., 2021a, b). These larger landforms provide evidence of spatio-temporal variation in thermodynamics such as basal thermal boundaries, ice flow velocities and directions, and meltwater routing, all of which affect ice sheet configuration, as well as the timing and rates of ice retreat (e.g. Knight et al., 1999; Greenwood and Clark, 2009a, b; Storrar et al., 2014; Margold et al., 2015). However, where these larger landforms are not identified (i.e. because they did not form, or because they have been partly or

* Corresponding author.
*E-mail address:* c.delaney@mmu.ac.uk (C.A. Delaney).

https://doi.org/10.1016/j.quascirev.2023.108041

completely removed by later erosion) the pattern of ice sheet deglaciation can be more difficult to decipher.

One solution is to examine smaller, low amplitude glacial landforms, generally <15 m high, of limited lateral extent, and normally only identifiable on digital elevation models with resolutions of <5 m per pixel, to elucidate local ice sheet behaviour (e.g. Evans et al., 2014, 2021; Delaney et al., 2018). These features include: (i) minor ribbed moraine (e.g. Möller and Dowling, 2015; Putņins and Henriksen, 2017); (ii) ice-marginal and sub-marginal moraines (e.g. Ojala, 2016; Chandler et al., 2020); (iii) crevasse-squeeze ridges (CSRs, e.g. Sharp, 1985; Bennett et al., 1996; Andreasson et al., 2014; Evans et al., 2016b; Delaney et al., 2018); (iv) glaciofluvial hummocks (e.g. Peterson and Johnson, 2017; Lewington et al., 2020); (v) mini-drumlins and MSGL remnants (e.g. Dowling et al., 2016; Delaney et al., 2018); and (vi) low relief hummocks and ridges that are included within the 'umbrella' designations of hummocky topography, hummocky terrain and hummocky moraine (e.g. Hoppe, 1952; Benn, 1992; Attig and Clayton, 1993; Hambrey et al., 1997; Eyles et al., 1999; Boone and Eyles, 2001; Benn and Evans, 2010; Evans et al., 2014, 2021; Möller and Dowling, 2015; Delaney et al., 2018). The latter category of low relief hummocks and ridges is the focus of this study. The terms 'hummocky moraine', 'hummocky terrain' and 'hummocky topography' have often been used indiscriminately within the literature. Here, we use the term hummocky topography to incorporate all three terms and to refer to areas of low relief (<15 m), mounded, irregular landforms underlain by diamictons and sand and gravel.

Previous studies indicate that the landforms found within hummocky topography are extremely varied, and include linear ridges (e.g. Benn, 1992; Hambrey et al., 1997; Evans, 2009; Evans et al., 2014, 2016b, 2021; Cline et al., 2015; Delaney et al., 2018) and hummocks or mounds, with and without a central depression (e.g. Johnson et al., 1995; Eyles et al., 1999; Boone and Eyles, 2001; Evans et al., 2014, 2021) and these features are often arranged with a preferential alignment (e.g. Benn, 1992; Hambrey et al., 1997; Lukas, 2005; Benn and Lukas, 2006; Evans, 2009; Evans et al., 2014, 2021; Möller and Dowling, 2015). These hummocky tracts are interpreted to have formed under a wide range of glacier/ice sheet thermodynamic and ice flow conditions, in both subglacial and supraglacial positions. Hummocky topography is a common feature of palaeo ice sheets, but has not always been used for detailed ice sheet reconstructions, as it may be difficult to identify in the field or on low-resolution aerial photographs, especially in well-vegetated areas with complex histories of agricultural landuse. In addition, sediment exposures through hummocky topography (which are relatively rare) are often widely spaced and two-dimensional, so the relationship between geomorphology, sediment composition and landform structure is often unclear. Consequently, the conditions under which hummocky topography was created are debated (see Benn and Evans, 2010 for a discussion of models of hummocky terrain and hummocky moraine formation). However, recent advances in non-destructive, high-resolution morphological and sedimentary techniques, and in particular in the use of LiDAR-generated, hillshaded DEMs, now allow detailed examination of the low-amplitude glacial landforms that form hummocky topography (e.g. Evans et al., 2014; Möller and Dowling, 2015; Peterson et al., 2017; Delaney et al., 2018; Chandler et al., 2020). By mapping the spatial variability of hummocky topography and combining it with detailed morpho-sedimentary analyses, these landforms can provide crucial diagnostic information for reconstructing shifting basal thermal conditions, ice flow velocities and directions, and basal meltwater distribution during ice retreat (e.g. Evans et al., 2014; Peterson et al., 2017; Delaney et al., 2018).

In this paper, we combine airborne LiDAR (Light Detecting and Ranging), high-resolution aerial photography, Ground-Penetrating Radar (GPR), and sedimentological analyses (including micromorphology) to investigate the three-dimensional structure of hummocky topography in central Ireland, an area where the position of the last Irish Ice Sheet (IIS) margin and the spatial and temporal retreat pattern of the IIS is under debate (Warren, 1992; McCabe, 2008; Clark et al., 2012). Our aim is to determine the processes involved in the construction of hummocky topography and establish the glacial conditions during IIS recession across the area. Our results indicate that hummocky topography: 1) records spatially variable subglacial and ice-marginal ice and meltwater dynamics during IIS recession; 2) enables accurate reconstruction of ice recession trajectories where larger landforms do not; and 3) may be a valuable component in other palaeo ice sheet reconstructions.

## 2. Regional topography, glacial landform distribution and palaeoglaciological models

The central Irish Midlands around the Brosna River basin (referred to as the Brosna basin below) is a low-relief plain (~40–70 MOD, meters above ordnance datum) which drains westward through the Brosna River and its tributaries to the River Shannon and is underlain by Carboniferous limestone, with inliers of Palaeozoic sedimentary rocks (Sevastopulo and Wyse-Jackson, 2009). These inliers form ridges of higher ground extending southwest across the area (e.g. Knockdomny; Fig. 1). Apart from these hills, glacial landforms are the most prominent topographic features, with glacial and post-glacial deposits masking bedrock almost everywhere. Much of the area is covered by Holocene peat and alluvium. These are underlain by glaciolacustrine silts and clays which were deposited in proglacial Palaeolake Riada, an ice-contact lake that formed when ice retreated westward and northwestward down a reverse slope during the Last Glacial Termination (LGT; Pellicer et al., 2012; Delaney, 2022).

Mapping by the Geological Survey of Ireland (2017) indicates that the northern margin of the basin, the area discussed here, is underlain by limestone-derived tills, with sandstone till occurring adjacent to Devonian sandstone outcrops. The eastern part of the area is more sedimentologically variable, with gravels underlying esker ridges, and extensive areas of hummocky sand and gravel deposits interspersed with lake deposits and Holocene peat and alluvium.

### 2.1. Glacigenic Landforms

*Glaciofluvial and glaciolacustrine landforms – eskers and flat-topped mounds:* these are the most prominent glacial landforms in the area, first mapped by Sollas (1896) and most recently by the Geological Survey of Ireland (2017). The eskers are discontinuous ridges (<200 m to >20000 m long, 50–500 m wide) and are underlain by conduit and channel fill deposits, commonly leading downstream to fan-shaped or flat-topped areas underlain by well-sorted sediments (Fig. 1; Flint, 1930; Delaney, 2002b, 2002a, 2002b, 2022; Pellicer et al., 2012; Delaney et al., 2018). The northern part of the basin, the main study area considered here, is bound by three large eskers, the Moate and Horseleap eskers to the north and the Eiscir Riada to the south. All are multi-crested ridges underlain by boulder, cobble and pebble gravels with sedimentary structures indicating transport eastward and southeastward. Flat-topped areas at their downstream end are underlain by Gilbert-type deltaic sediments formed at the point of discharge into Palaeolake Riada (Fig. 1; Pellicer et al., 2012; Geological Survey of Ireland, 2017; Delaney, 2019, 2022). The Eiscir Riada has been interpreted as an interlobate feature, marking the boundary between a southeastward flowing lobe to the north and an eastward flowing lobe to

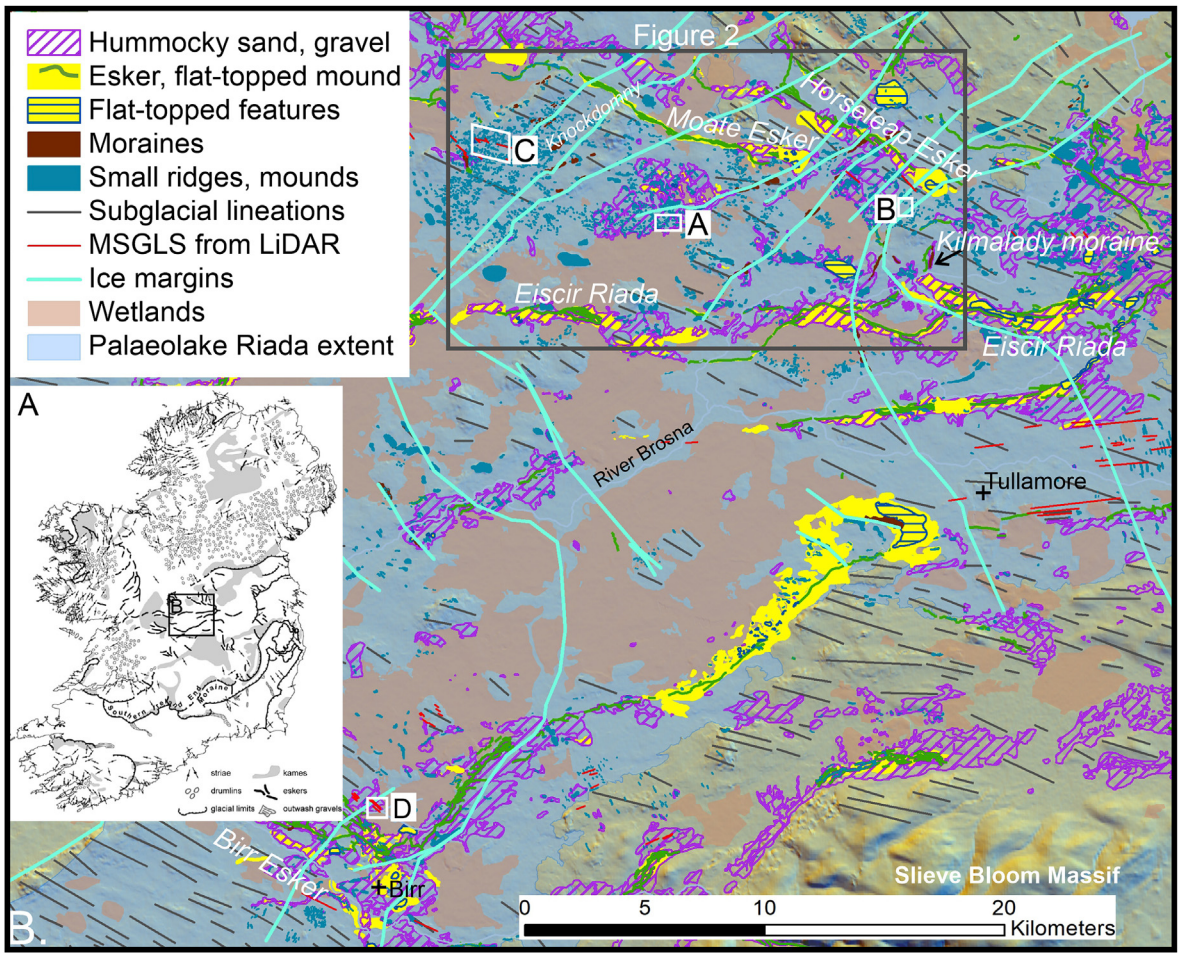


**Fig. 1.** A. (inset): Map of glacial landforms in Ireland, showing location of the study area. After Synge (1979). B. Map of the study area, showing major glacial landforms, including subglacial lineations and eskers, and position of sites. Hummocky sand and gravel, eskers, flat-topped mounds and wetland areas from the Geological Survey of Ireland Quaternary mapping (Geological Survey of Ireland, 2017). Moraines, small ridges and mounds, MSGLs from LiDAR and ice margins from Delaney (2022).

the south (Pellicer et al., 2012). It forms part of a major eastward draining esker system, the Midlands system (McCabe, 2008). In the southwest of the Brosna basin, this system is succeeded, and partly overlain by, a southeastward draining esker system consisting of multiple small, single-crested esker ridges underlain by poorly sorted gravels. One esker, the Birr esker, widens downstream into a multi-crested, fan-shaped area interpreted as a supraglacial channel complex (Fig. 1; Delaney et al., 2018). Separate to the eskers, flat-topped mounds underlain by deltaic sediments also occur and are interpreted as ice-contact deltas formed at point discharges into a large proglacial lake (Fig. 1; Gallagher et al., 1996; Pellicer et al., 2012; Delaney, 2019; 2022).

*Subglacial Lineations:* These features are uncommon within the Brosna basin. Drumlins, MSGLs and crag-and-tails occur along the northern margin, indicating southeastward ice movement (Fig. 1; Greenwood and Clark, 2009a, b; Geological Survey of Ireland, 2017), while lineations in the central and southern part of the Brosna basin suggest an ESEward ice flow direction (Fig. 1). However, MSGLs mapped using newly available 1 m resolution LiDAR DEMs (in red on Fig. 1) indicate a change from southeastward to ENEward ice flow along the southern margin of the Brosna basin, so ice flow direction is not well constrained in this part of the basin.

*Moraines:* These are also rare within the Brosna basin. North of the Eiscir Riada, the Kilmalady moraine (Fig. 1), mapped by Pellicer et al. (2012), is interpreted as an ice-marginal push moraine associated with a local readvance from the northwest (Delaney, 2019). Further ice-flow transverse ridges west of this, aligned with ice-contact deltas, indicate a retreating ice margin aligned NE-SW around the Moate and Horseleap eskers (Fig. 1; Delaney, 2019, 2022).

*Hummocky topography*: this is common throughout the Brosna basin and is considered to be underlain by sand and gravel and closely associated with esker ridges (Fig. 1; Geological Survey of Ireland, 2017). Hummocky topography in the Irish Midlands was originally interpreted as an ice-marginal feature formed within a stagnant marginal zone during steady ice recession (e.g. Charlesworth, 1928; Flint, 1930; Farrington and Synge, 1970). However, recent mapping using high-resolution satellite imagery and LiDAR DEMs shows that some areas of hummocky topography contain multiple small (<10 m high) ridges and mounds aligned roughly transverse to the ice flow direction as indicated by lineations and eskers (Fig. 1; Delaney et al., 2018; Delaney, 2022). In the southern part of the Brosna basin LiDAR DEMs indicate that the hummocky topography is composed of fragmented MSGLs reworked into crevasse-squeeze ridges (CSRs) and was therefore generated subglacially (Delaney et al., 2018). These overprinted landforms provide evidence for at least two phases of accelerated ice flow and subsequent stagnation during IIS recession in the southern Brosna basin and therefore a more dynamic ice recession regime than previously suggested (Delaney et al., 2018; Delaney,

2019). Consequently, the interpretation of hummocky topography as an ice-marginal stagnation feature may not be correct.

### 2.2. Existing reconstructions of deglaciation

The rarity of moraines and subglacial lineations within the Brosna basin means reconstructions of ice margin positions during the recession of the last IIS have relied heavily on esker orientation and ice-contact glaciolacustrine features (deltas and subaqueous outwash fans) (Charlesworth, 1928; Farrington and Synge, 1970; Warren, 1992; Delaney, 2002a, 2001; McCabe, 2008; Pellicer et al., 2012). This has led to conflicting models for ice dynamics and ice sheet configuration during the LGT (e.g. Warren, 1992; McCabe, 2008). However, more recent work has combined multiple evidence threads, including lineation orientation, moraine and ice-flow transverse ridge alignment with glaciofluvial and glaciolacustrine features (Fig. 1; Greenwood and Clark, 2009b; Clark et al., 2012; Delaney et al., 2018; Delaney, 2019, 2022). Most recently, Delaney (2022) has suggested that small moraines within hummocky topography in the northern part of the basin (around Sites A, B and C; Fig. 1) can be correlated with further groups of ridges between the northern Brosna basin and the Irish Sea, and with moraines in Dundalk Bay on the Irish Sea coastline. These are thought to have formed during and after a radiocarbon-dated regional readvance, the Killard Point Readvance (17.4 ± 0.3 ka cal BP; McCabe et al., 2007; Chiverrell et al., 2013, 2018). Despite these regional observations, the origin of the hummocky topography is unclear but may provide important insights into regional ice recession patterns and is therefore the basis for this study (Delaney et al., 2018). Hence, we report here on a high-resolution examination of the characteristics of hummocky topography and demonstrate how it can be used to improve models of ice sheet regional dynamics during deglaciation in this part of Ireland.

## 3. Methods

We focus on the central Irish Midlands immediately north of the Eiscir Riada (Fig. 1; Charlesworth, 1928; Warren, 1992; McCabe, 2008; Pellicer et al., 2012), an area selected on the basis of availability of newly available, high-resolution (1 m resolution) LiDAR DEMs covering areas of hummocky topography. Minor ridges and mounds within the area have been mapped previously, but not examined in any detail (Delaney, 2022). After initial mapping of a large zone of hummocky topography, three smaller, geomorphologically representative areas (Sites A, B, C; Fig. 1) were selected for further geomorphological and sedimentological study. We examined ridges (Ridges A1-3 at Site A, Ridges C1-2 at Site C) and mounds (Mounds B1-4 at Site B) to reconstruct formation processes. For comparison, we examined a further site in the southwest of the Brosna basin (Site D; Fig. 1) where previous work on LiDAR DEMs provides evidence for possible formation mechanisms of hummocky topography (described above; Delaney et al., 2018).

### 3.1. Geomorphological mapping

Large landforms (>15 m high) were mapped using aerial photographs and the ALOS PALSAR Radiometric Terrain Corrected (RTC) high-resolution multi-directional hillshaded DEM (12.5 m resolution; ASF DAAC, 2007), processed using Relief Visualization Toolbox (RVT; Kokalj and Somrak, 2019; Zakšek et al., 2011). Mapping of small-scale (<5 m), low-amplitude landforms had previously been carried out (Delaney, 2022) using vertical aerial photographs from two sources: (i) the ArcGIS World Imagery (Clarity) tile layer (ESRI, 2022); (ii) historical aerial photographs available through Google Earth Pro. These were supplemented for this study using airbone LiDAR DEMs (collected by Transport Infrastructure Ireland and downloaded from the Geological Survey of Ireland data portal) and multi-directionally hillshaded using RVT. Mapping was verified by field surveys.

### 3.2. Sedimentology and micromorphology

Sedimentological descriptions were undertaken at the macro- and micro-scale, in order to identify depositional processes during landform formation. Sediment exposures are rare apart from in sand and gravel extraction pits in the study area, and a total of six exposures in ridges and mounds were found during field survey. Five small exposures, all <8 $m^2$ in area, were described and logged (Fig. 2). At Site A, an exposure 20 m long and up to 4 m high (the largest exposure in the area) was selected for further analysis and sediments were logged. The sediments in the exposure are well-cemented owing to an abundance of calcium carbonate derived from limestone-dominated till and are also compacted, so clast fabric measurements were limited to Lithofacies 3 (LF 3), which dominates the western side of the ridge (see below). The resulting data were plotted and eigenvalues calculated using Stereonet 10.0 (Allmendinger et al., 2013). LF 3 was also sampled for micromorphological analysis. Due to cementation, micromorphological samples could not be collected using kubiena tins (van der Meer, 1995). Instead, one large (~30 × 20 × 20 cm), sediment sample block was carved out from LF 3 (see below), in an area considered representative of the lithofacies. The sample was acetone-dried and resin-impregnated and three thin sections (lower, middle and upper) were produced following standard procedures (Lee and Kemp, 1993; Carr and Lee, 1998; Menzies, 2000; Palmer et al., 2008). All thin sections were examined using a Leica © Z6 APO petrological microscope with a rotating stage (5.7-36× magnification). Descriptions follow classifications developed by Brewer (1976), van der Meer (1993), Menzies (2000) and Linch et al. (2012). Grain roundness follows the classification of Powers (1953). Thin sections were aligned with the top edge of the slide horizontal relative to ground surface, so clast orientations are given as dip angles relative to the horizontal, to facilitate comparison with the macro-sedimentological clast fabric. It should be noted that, unless otherwise stated, all textural/structural measurements from this point forward reflect 'apparent' a-axes values as a consequence of the plane of slicing of the sample block during cutting.

### 3.3. Ground-penetrating radar (GPR)

GPR was used to identify major changes in composition and structural features within the landforms. GPR surveys were carried out using a Pulse EKKO PRO LF (low frequency) system. A preliminary survey of small exposures through the field area indicated that sediment was predominantly diamictic and contained silt and clay, suggesting that the radar pulse would likely be attenuated (Jol and Bristow, 2003). Survey parameters were designed to prioritise penetration depth over resolution in order to maximise the signal of major reflections and discontinuities (Jol and Bristow, 2003). Appropriate survey sites were selected on the basis of representative geomorphology and access. Data was collected using a perpendicular-broadside step survey, with 50 MHZ antennae at 2 m spacing, with a 0.5 m step size and a 450 ns time window. Initial processing included removal of bad traces and time zero adjustment, followed by application of DEWOW. Radar velocities were obtained by matching hyperbolae to point diffractions in the profiles (Neal et al., 2002). Traces were migrated accordingly and an automatic gain control (AGC) was applied. All profiles exhibited strong parallel reflectors so background removal was applied using

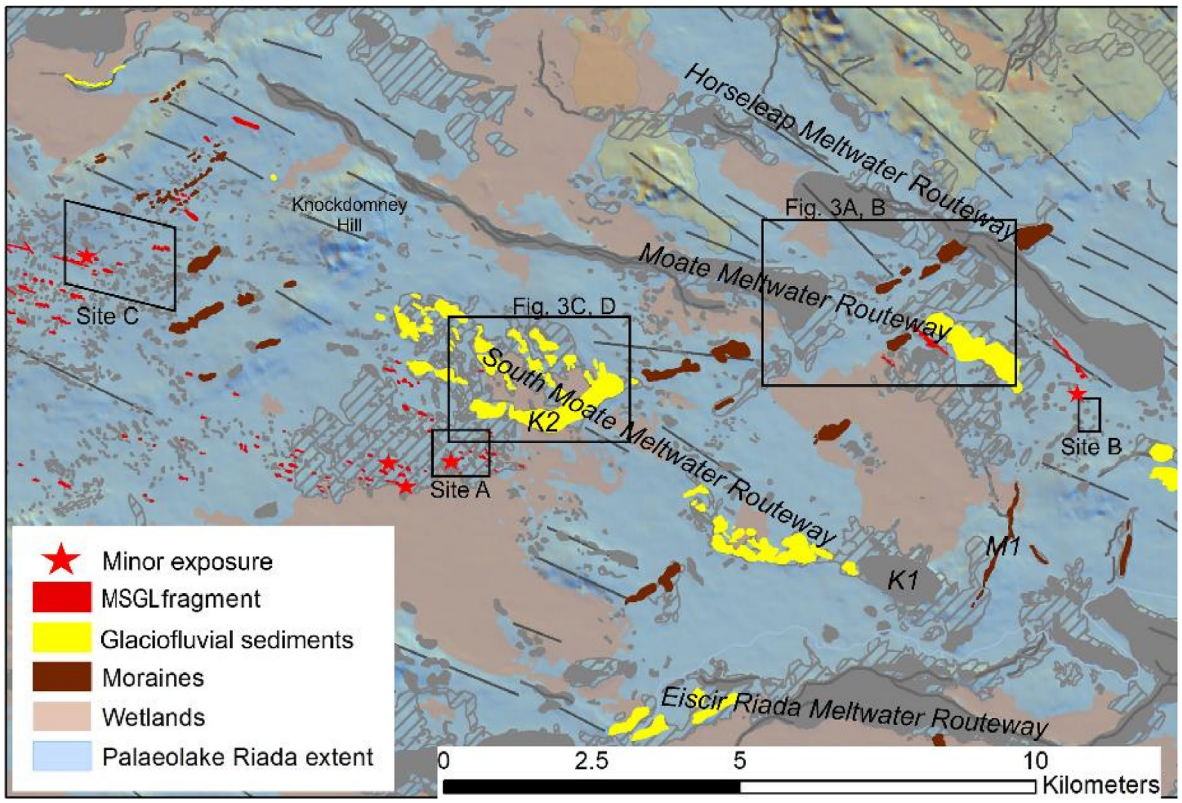


**Fig. 2.** Map of main research area, showing distribution of Quaternary sediments and low amplitude ridges and mounds mapped for this study. Location of sites discussed in text and position of LiDAR DEM is shown.

a full length filter, to remove air and ground wave reflectors.

## 4. Results

### 4.1. Geomorphology

Mapping results for the main field area (around Sites A, B and C) are shown in Fig. 2. The area around Site D was mapped previously (Fig. 1; Delaney et al., 2018), but significant features from this site are included in the description below. The following landforms were identified:

#### 4.1.1. Glaciofluvial and glaciolacustrine landforms - eskers and flat-topped mounds

Previously mapped features are shown in grey on Fig. 2. We identified several additional new glaciofluvial/glaciolacustrine features (Fig. 2). Beyond the terminus of the Moate esker, a raised linear zone of ridges and mounds (up to 10 m high, 700 m wide) trends ESE parallel to the Horseleap esker (Figs. 2 and 3A, B) and contains multiple small borrow pits, indicating that the glacial meltwater routeway (MR) marked by the Moate Esker continues further southeast than previously suggested. A second raised linear zone of short, sinuous ridges (<400 m long) and mounds (up to 15 m high, 700 m wide), also with borrow pits, extends WNW from a previously mapped ice-contact delta (K1 on Fig. 2; Pellicer et al., 2012) and indicates the location of a further MR (called the South Moate MR here) parallel to the Moate and Horseleap Eskers (Fig. 2; 3C, D). Northwest of this group of features there is a gap of 3 km, before a prominent, elongated, partly flat-topped mound (length 3500 m, width 500 m, height 15 m; K2 on Fig. 2; 3) marks the next part of the South Moate MR. The long-axis of this feature is oriented northeast-southwest, sub-parallel to moraines and an ice-contact delta to the northeast. North of mound K2 is a series of parallel short, sinuous ridges (2–6 m high, 50–100 m wide, 400–800 m long; Fig. 2; 3C, D) and smaller mounds (200–500 m wide, 5–15 m high) with flat or gently sloping surfaces leading to mound K2. Small exposures in several of these mounds (Fig. 3C and D) show they are composed of well-sorted silts, sands and gravels, which is consistent with glaciofluvial deposition. In one flat-topped mound (K3 on Fig. 3C, D), a larger exposure reveals cross-stratified, matrix-rich pebble gravels interbedded with massive and normally graded fine, silty sand and clay laminae dipping south and southeast, that are interpreted as glaciodeltaic foresets. The associated sinuous ridges are more mixed in sedimentological composition – some were previously mapped as sand and gravel (GSI, 2017), while we have observed diamicton in others, similar to ridges further south around Site A. The LiDAR DEM indicates that some of these ridges are overlain by mounds underlain by sand and gravel.

The three MRs are closely spaced, with a gap of 2–5 km between the South Moate MR and the Moate MR, and <2 km between the Moate and Horseleap MRs for much of their length.

#### 4.1.2. Hummocky topography

Previous mapping indicates that much of the study area consists of a mixture of low ridges and mounds, many of which are aligned (3–8 m high, 50–100 m wide, 100–200 m long; Fig. 2; Delaney, 2022). Further mapping and measurement using LiDAR DEMs provides more detail on these features. We identified mounds (length:width elongation ratio <2) arranged in groups oriented both parallel and at a high angle to the dominant ice flow direction, as inferred from drumlins and MSGLs (Greenwood and Clark, 2009a, b; Geological Survey of Ireland, 2017; Figs. 1 and 2). Ridges (elongation ratio 2–4) are generally oriented at a high angle to the inferred ice flow direction. In plan view, many ridges have lower

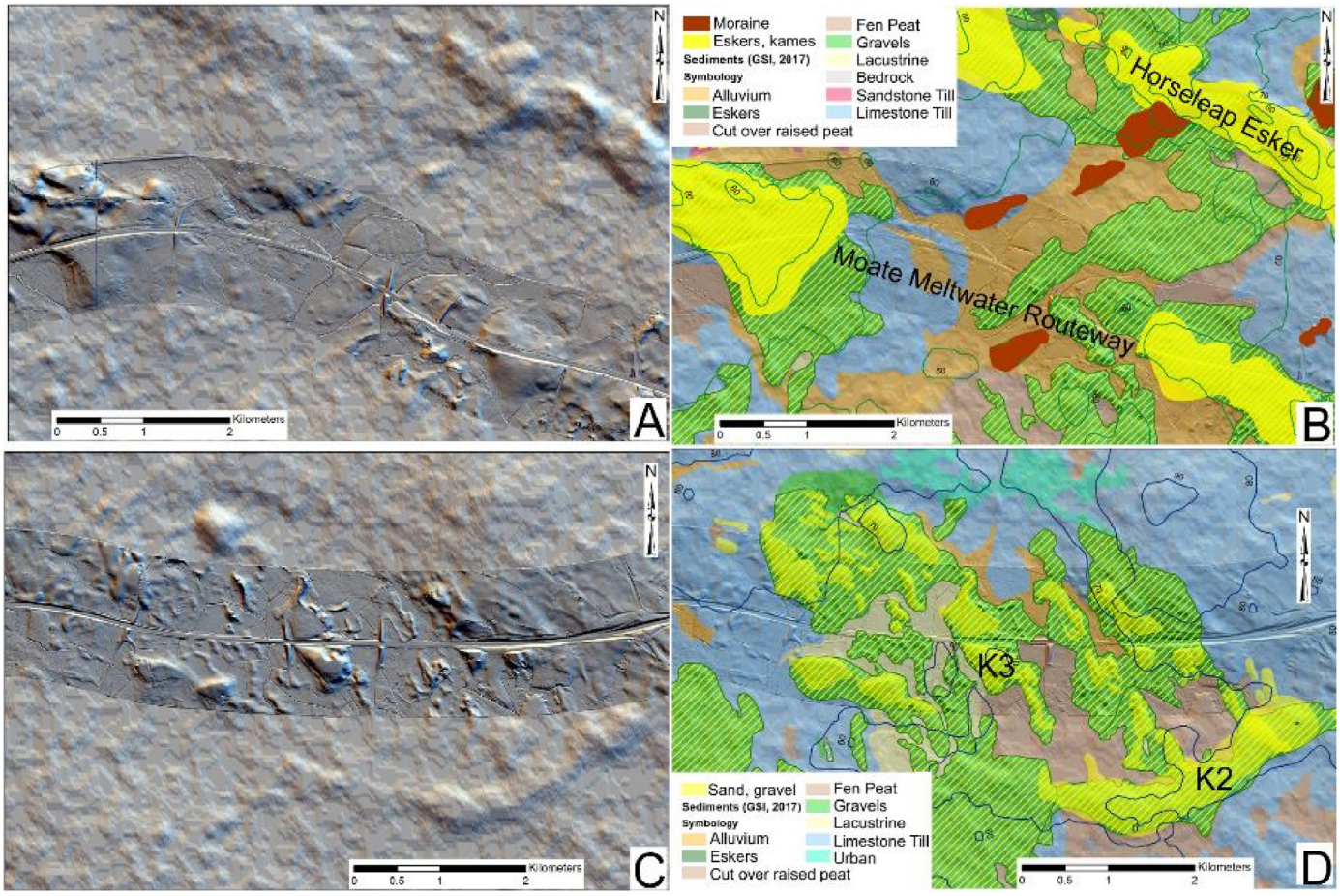


**Fig. 3.** A. Combined LiDAR and radar hillshaded DEM of the area between the Mount Temple and Horseleap eskers, showing the flat-topped terminus of the Mount Temple esker, moraines, areas of unaligned mounds in hummocky topography. B Interpretation – diagonal yellow lines indicate areas mapped as 'hummocky' by the GSI (2017). C. Combined LiDAR and radar hillshaded DEM of the northwestern part of South Moate Meltwater Routeway (MR) around Moate. D. Interpretation of DEM. K2 and K3 are flat-topped mounds mentioned in the text; K1 is shown in Fig. 2.

extensions at a high angle to the main ridge crestline; i.e. parallel to ice flow (Fig. 4A and B). Crestlines are often undulating, with higher points corresponding to the location of ridge extensions separated by saddles along the ridge crest. However, flat-topped ridges also occur. Many ridges are asymmetrical in cross-profile, with longer, gently sloping ice-proximal slopes and shorter, steeper ice-distal slopes. Ridge spacing and individual ridge width is similar (50–200 m).

Three sites dominated by ridges, Sites A, C and D (Fig. 2) were chosen for further study. Sites A and C lie south of the South Moate MR at the eastern and western ends of a group of ridges with associated mounds. At Site A, NNW-SSE and WNW-ESE oriented ridges and aligned mound groups have undulating crestlines and in places appear streamlined on aerial photos (no LiDAR was available for this area; Fig. 4A). Ridges do not align laterally, and do not appear to be the fragmented remains of more continuous features. Along the southern margin of the area, a cluster of WNW-ESE oriented ridge segments are generally shorter and narrower than the NNW-SSE ridges, but of similar height (widths 48 m vs 91 m, respectively; lengths <100 m vs 100–300 m, respectively), and appear streamlined (Fig. 4A).

Hummocky topography at Site C consists of mounds, ridges and hollows with preferred alignments (Fig. 4B–E). Ridge crestlines are dominantly oriented NE-SW (transverse to the ice flow direction inferred from MSGLs in the surrounding area) with secondary orientations at WNW-ESE and NNE-SSW (Fig. 4B and C), while elongate depressions and saddles between high points along ridges are mostly oriented WNW-ESE, parallel to ice flow, with a secondary NE-SW alignment (Fig. 4B and C). As at Site A, the largest, NE-SW aligned, ridges (heights 3–5.5 m, widths 90–150 m, lengths 100–350 m) have undulating crestlines, with high points where they intersect with ridge extensions. However, unlike Site A, crestlines of ice flow-transverse ridges are straight in plan view, and crestlines often align from ridge to ridge, giving the impression that some ridges (but not all) may be the remnant of a more continuous ice flow-transverse feature (Fig. 4B). Flat-topped ridges are also common. A secondary set of WNW-ESE ridges also occurs at Site C, but these are lower than at Site A (1–3 m at Site C vs. 3–8 m height at Site A). Linear groups of mounds also aligned WNW-ESE occur, as well as low extensions from the main NE-SW oriented ridges (Fig. 4D and E).

Site D lies 30 km south of the main study area, in hummocky topography adjacent to the Birr esker (Fig. 1; Delaney et al., 2018). The glacial deposits here consist of multiple short ridges and parallel grooves displaying multiple orientations with a dominant orientation transverse to ice-flow, as indicated by nearby MSGLs. Ice flow-parallel ridges and grooves extend into MSGLs to the NE, while further small ridges are oriented N–S, at a high angle to ice flow direction (Delaney et al., 2018).

A further site, Site B, was selected to examine non-oriented

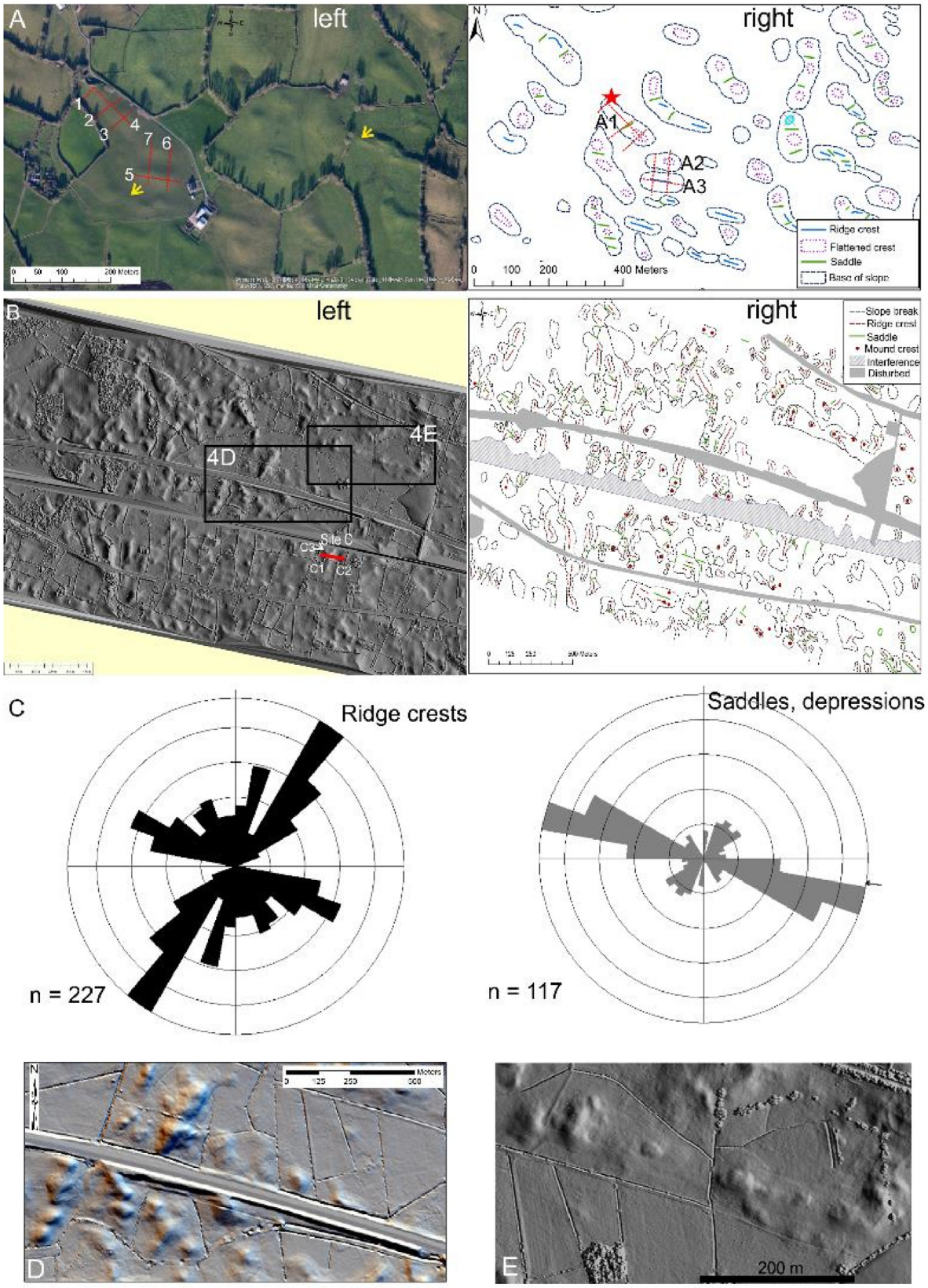


**Fig. 4.** A. Left: air photo of Site A, showing ridges and mounds and position of GPR profiles (red lines). Yellow arrows mark position of fragments of MSGLs. Right: schematic map of Site A topography, showing Ridges A1, A2 and A3, position of GPR survey lines (red) and position of exposure in Ridge 1 (red star). B. Left: LiDAR DEM of Site C, showing position of ridges A1-C3, GPR line and Fig. 4D and E. Right: schematic map Site 3 topography. C. Rose diagram of ridge and saddle orientations at Site C. D. Close-up of LiDAR DEM of ridges at Site C, showing ice-flow transverse ridges overlying a fragmented MSGL. E. Close-up of fragmented MSGL at Site C.

hummocky topography. The site lies immediately south of the Horseleap Esker and between the southern terminus of the Moate Esker and further accumulations of sand and gravel identified to the east (Fig. 2). The topography consists of low mounds with an irregular plan form with no obvious elongation. Mounds are both flat-topped and slightly domed.

### 4.2. Sedimentology

#### 4.2.1. Ice flow-transverse ridges – macroscale sedimentology

Small exposures in the area around Sites A and D (areas <8 $m^2$; locations on Fig. 2) indicate that ridges are composed of a clast-rich diamicton with a silty matrix containing blocky, sub-angular to sub-rounded clasts. Ridges become increasingly clast-rich with depth and discontinuous, crude, clast-rich horizontal stratification is occasionally visible on the ice-distal side of ridges and at the base of deeper exposures (see below).

Around Site C, diamicton exposed in a 4 $m^2$ section also has a silty matrix and contains blocky, sub-angular to sub-rounded, limestone clasts up to boulder size. Clasts are commonly fractured and clusters of clasts are common.

The largest exposure found lies at the northern end of Ridge A1 (Fig. 4). Three sedimentary lithofacies are visible (Fig. 5). At the northern end of the exposure Lithofacies 1 (LF 1), which directly underlies Lithofacies 3 (LF 3), is characterised by 0.4 m thick, highly compacted diamicton, with a variable matrix of silt and occasional patches of silty sand (Fig. 5). It contains pebble to boulder-size particles of muddy limestones and shales. LF 1 is separated from the overlying LF 3 by a distinct horizon of openwork pebbles and cobbles, picked out by a poorly developed iron pan, with the occurrence of iron staining below this layer.

The contact between LF 1 and higher LF 2 is not visible at this site as LF 2 thins from at least 1 m thick under the ridge crest to disappear as LF 3 thickens under the western (ice-proximal) slope of the ridge; however, as LF 2 is topographically higher than LF 1 it is likely that it overlies LF 3 under the ice-distal side of the ridge. LF 2 consists of crudely and indistinctly stratified, matrix-to clast-supported diamicton with matrices of clay-rich silt to coarse sand, supporting sub-angular to sub-rounded boulders, cobbles and pebbles. Stratification is created by a combination of matrix-rich areas interspersed with horizons of weakly imbricated, openwork cobbles, and occasional lenses of coarse sand or silty fine sand. Bedding is discontinuous and best developed at the eastern end of the section, under the crest and eastern slope of the ridge, where the bed is thickest. Here the apparent dip of the bed is east (toward 080°E; dip c. 10°; Fig. 5); imbrication is west to WSW. The contact between LF 2 and the overlying LF 3 is irregular and poorly defined (Figs. 5 and 6C). Immediately east of the crest of the ridge, the contact between the two lithofacies undulates at up to 0.6 m amplitude, but dips parallel to the surface under the ice-proximal face (westward facing slope) of the landform (Fig. 6C).

The uppermost LF 3 is wedge-shaped and less than 1 m thick and discontinuous under the ridge crest, but thickens rapidly to over 4 m thick under the southwest slope of the ridge. It consists of a very stiff, compacted and cemented, clast-rich, matrix-supported diamicton, with a variable matrix of sandy silt (approximately 40% sand, 60% silt and <1% clay; light brownish grey (2.5 Y 6/2) to dark greyish brown (2.5 Y 4/2)). Clasts are angular to subangular limestone, shales and sandstones ranging from millimetre-size to boulders (up to 0.5 m a-axes). Clasts become increasingly angular upward through the section. The diamicton is generally massive, but in places bands of higher fissility, clast-rich horizons, clusters of often imbricated, angular fractured clasts and alignment of a-b planes of fractured clasts give a sense of partings or planes within the lithofacies. These appear to dip westward, roughly parallel to the ridge surface slope (apparent dip; Figs. 5 and 6A). A well-developed clast fabric is visible, with clasts dipping in the same direction as structural planes. Clast fabric measurements display unimodal clustering with dip WSW overall (Fig. 5; V1 trend 238.6° SW, plunge 21.6°; S1 = 0.6948, S2 = 0.2095, S3 = 0.0957; isotropy index 0.14, elongation index 0.6985), parallel to the observed planes. Isolated, irregular lenses (up to 0.1 m thick, 0.4 m long) of medium to coarse sand, silty sand, and silt-sand-granule mixes occur within the matrix and increase in abundance downward through the lithofacies and from the proximal to the distal side of the ridge. These inclusions are sometimes crudely laminated (laminae ~5 mm thick).

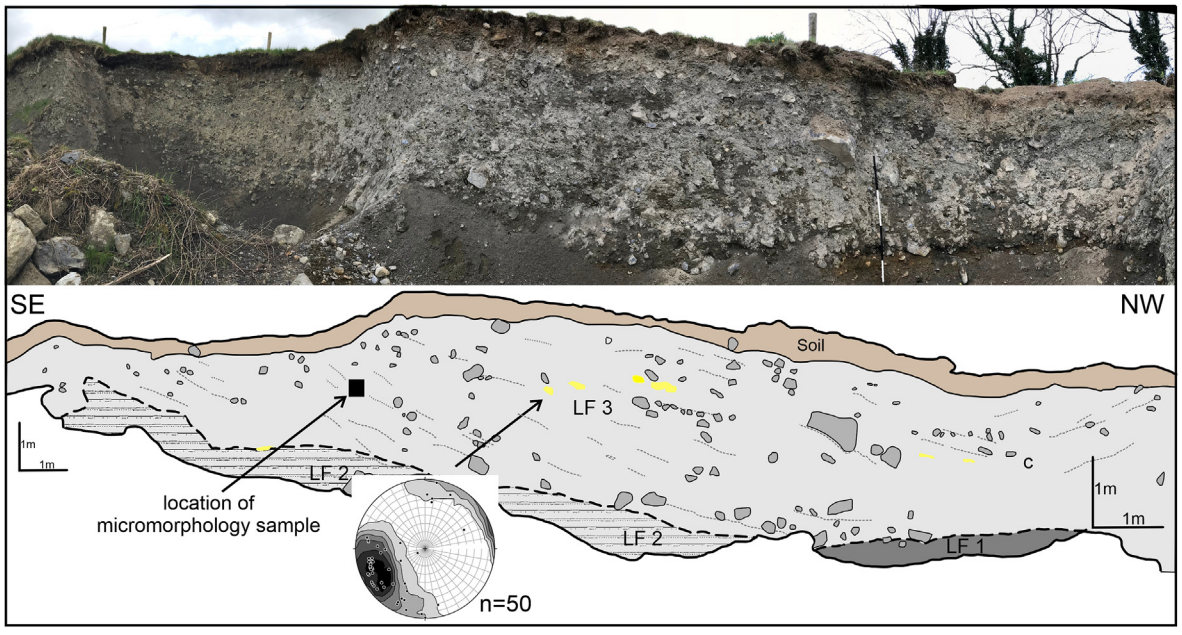


**Fig. 5.** Exposure in sediments underlying Ridge A1. Eigenvalues for clast fabric: S1 = 0.6948; S2 = 0.2095; S3 = 0.0957.

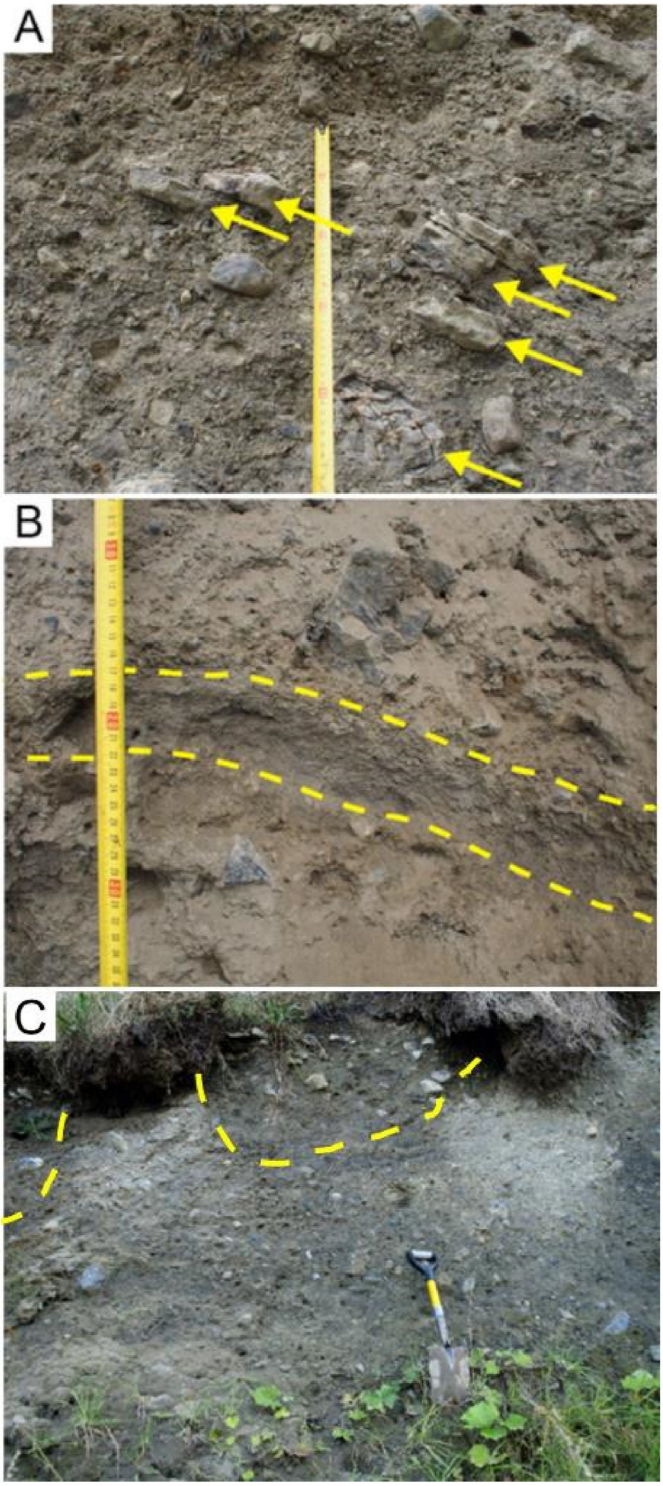


**Fig. 6.** Diamictons underlying Ridge A1, central Irish Midlands: A) Flat, imbricated clasts dipping toward ~310° in LF 3; B) Horizontally laminated sand lens toward the base of LF 3. C) Crudely stratified sediments underlying the ridge crest in LF 2, partly overlain by LF 3, which is present as blocks at the top of the section, appearing as wetter areas in the photo. The contact between the two lithofacies is indicated by the yellow dashed line. LF 2 sediments consist of stratified diamicton formed by areas of clast-rich and clast-poor sediment and discontinuous lenses of silty sand. Beds dip gently to the north east (left of photo).

#### 4.2.2. Micromorphology

We focussed on LF 3 sediments for further study, as they dominate within the ridge. Three thin sections were examined (Fig. 5). Detailed descriptions are provided in Supplementary Information (Appendices, Text A1, Figs. A1, A2) and are summarised below. The dominant sediment in all thin sections comprises coarse-grained, clast-rich, matrix-supported diamicton with very angular to rounded, but dominantly sub-rounded skeleton clasts (300 μm - 20 mm in size; Fig. A1), generally evenly distributed through the sediment, with occasional clusters. Clasts typically exhibit dips of 30–50° from horizontal (Appendices, Fig. A2). The matrix (particles <30 μm in size; van der Meer and Menzies, 2011) is typically fine-grained and dense, and is generally distributed evenly, with occasional very fine clayey patches (Fig. 7A).

The diamicton is highly porous, with high to moderate abundances of simple packing voids (~100 μm to >2000 μm pores), channels (~1–4 mm in length) and planar jigsaw fissures, all with defined boundaries. Fissures and strings of interconnected, bubble-shaped pores crudely delineate the edges of some of the larger clasts (Fig. 7B). Straight lines of up to seven or more interconnected, 'bubble-shaped' pores are present in low to moderate abundance (Table 1). Voids, especially pores, are typically associated with accumulations of clay either within the voids themselves, along the perimeters of voids, or directly adjacent to voids (Table 1; Fig. 7C, J). In one case, clay-lined void/pore spaces cut across disaggregated laminations (Fig. 7D).

In one thin section, a fine-grained, banded zone – which gives a sense of flow – can be traced through the diamicton, composed of disaggregated, alternating, clayey, fine-grained silt and silty, fine-grained sand laminations with diffuse boundaries (~0.2–0.3 mm thick, dipping at 20–40° from the horizontal; Fig. 7E). This structure appears to be partly composed of primary laminations and partly of multiple domains and is folded with minor reverse faulting (Table 1).

Larger clasts are associated with sorting of fine-grained material in birefringent patches adjacent to clasts and as thin birefringent borders/lines of fine-grained material along clast boundaries (Table 1; Fig. 7F). This sorting may represent development of discrete (usually partial) 'clast haloes' (Linch et al., 2012; Linch and Dowdeswell, 2016).

Grain lineations are present in low to moderate abundance (Table 1; Fig. 7G). However, the long axes of grains that comprise these lineations are not always aligned parallel (in the direction of the lineation) as they should be in true grain lineations (Hiemstra and Rijsdijk, 2003). Partially destroyed clasts, identified as whole fossil particles released from nearby bioclastic fragments (Fig. 7H, are also present in low to moderate abundance, as are occasional crushed limestone grains (Table 1; Fig. 7I).

Intraclasts type III (~400 μm - 6.4 mm), composed of diamicton (Fig. 7J) or sand, are weakly to moderately developed and in low abundance (Table 1). Multiple domains are well-developed, in moderate to high abundance in all thin sections (Fig. 7K) and include patches of very fine-grained matrix adjacent to more clast-rich areas, as well as pockets of birefringent clay with diffuse boundaries. Finally, one well developed clay-filled hydrofracture running down the length of a large elongate clast is identified (Table 1; Fig. 7L). The only plasmic fabric identified is weak, linear birefringence on the upper and side boundaries of a few clasts, which here is described as skelsepic plasmic fabric (Table 1).

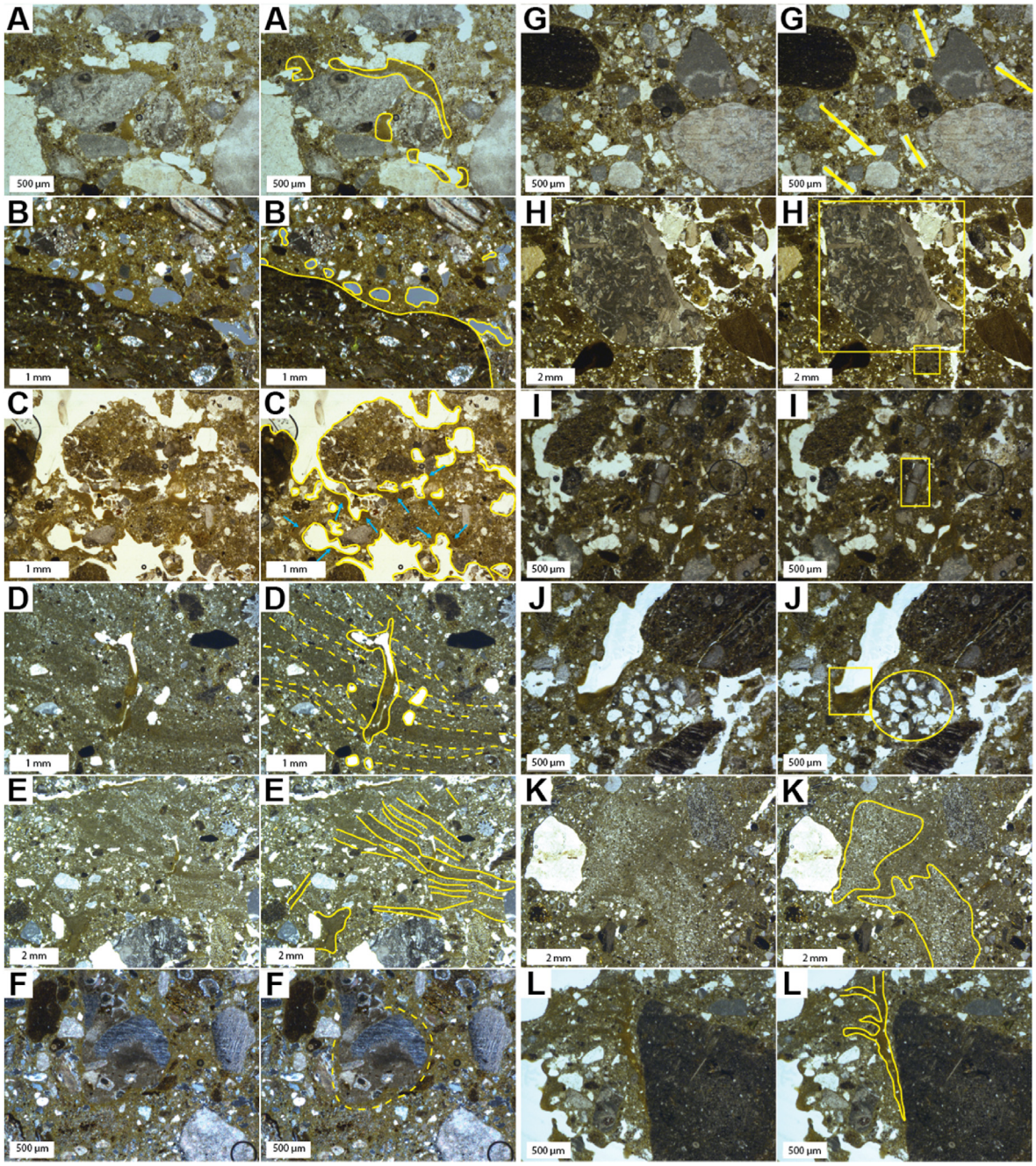


**Fig. 7.** Microstructures in LF 3, Ridge A1, central Irish Midlands. A. fine-grained pure clay matrix/domain patches. B. voids/pores delineating the upper edge of a large (>2000 μm) clast. C. pores (yellow lines) with associated clay accumulations/patches (blue arrows). D. clay-lined pores cutting across disaggregated laminations. E. disaggregated laminations of alternating clayey silt and silty sand, and a silty multiple domain (bottom left corner). F. sorting of fine-grained material around a (sub)rounded clast i.e. a 'clast halo'. G. grain lineations. H. whole fossil particle (small square) released from a nearby bioclastic fragment (e.g. large square). I. crushed grain. J. pore with associated clay accumulations (square), and a diamict intraclast type III (circle). K. fine-grained sand multiple domains adjacent to fine-grained silt multiple domains. L. clay-filled, branching hydrofracture.

### 4.3. Ground-penetrating radar

Radar profiles were measured at the four selected sites (A, B, C, D) described above. Ice-flow transverse ridges were examined at Sites A, C and D, and mounds at Site B.

#### 4.3.1. Ice-flow transverse ridges: Sites A, C, D

GPR profiles were measured across three ridges at Site A - a large ridge oriented at a high angle to the ice flow direction (Ridge A1) and two smaller, streamlined ridges with long-axes parallel to flow (Ridges A2 and A3; Figs. 8 and 9). This was supplemented by a single radar profile at Site C that traverses two ice-flow transverse ridges (Ridges C1 and C2; Appendices, Fig. A3) and one ice-flow parallel ridge, interpreted as an MSGL remnant (Ridge C3; Appendices, Fig. A3). A single radar profile at Site D traverses one ridge fully and is again oriented at right angles to the ridge long axis (Appendices, Fig. A4).

In the transverse ridges, the highest radar facies (RF B) consists of parallel, semi-continuous reflectors and is present in all profiles (Fig. 8; Appendices, Figs. A3, A4). A radar profile along the crestline

**Table 1**
Micromorphological structures in LF 3, Ridge A1, central Irish Midlands (Dm = Diamicton; La = Laminations; Rot/Comp = Rotation/Compression; P/dep = Post-depositional; PF = Plasmic Fabric; PW = Porewater; Sed. Mixing = Sediment Mixing; ◉◉◉ = High abundance, well-developed; ●●● = High abundance, moderately developed; ○○○ = High abundance, weakly developed; ◉◉ = Moderate abundance, well-developed; ●● = Moderate abundance, moderately developed; ○○ = Moderate abundance, weakly developed; ◉ = Low abundance, well-developed; ● = Low abundance, moderately developed; ○ = Low abundance, weakly developed).

| | | | Deformation Structures | | | | | | | | | | | | | | | | |
|---|---|---|---|---|---|---|---|---|---|---|---|---|---|---|---|---|---|---|---|
| | | | Rot/Comp/Slump | | Planar shear | | | | Abrasion | | Sed. Mixing | | PW | | PF | P/dep | | | |
| Thin section sample | Lithofacies | Section elements | Clast haloes/Sorting of fines around clasts | Folding | Reverse faults | Lines of bubble voids | Grain lineations | Partially destroyed clasts | Crushed grains | Intraclasts type III (Sediment) | Multiple domains | Hydrofractures/ Flow structures | Skelsepic | Fe/Mn staining | Voids with clay accumulations | | | | |
| Upper | Dm | | | | | ◉ | | ○ | | ○ | ◉◉ | | | ○ | ◉◉◉ | | | | |
| Middle | Dm | La | ○ | • | ○ | ◉◉ | ○ | ○ | ○ | ○ | ◉◉◉ | ◉ | | ○ | ◉◉◉ | | | | |
| Lower | Dm | | ●● | | | | ○ | ○ | ○ | • | ◉◉ | | ○ | ○ | ◉◉◉ | | | | |

of Ridge A1 indicates that RF B is thickest in saddles along the crest and under the lower ground on either side, but the highest reflector thins or disappears across the ridge high points (Fig. 8, Line 4). Along this radar profile multiple sub-vertical (angles >60°) discontinuities with displacement of reflectors across the discontinuity indicate faulting. Normal faults on either side of the higher parts of the ridge have displacements of up to 1 m. In contrast, under the ice-proximal slopes of this ridge, discontinuities dipping at between 20 and 50° indicate reverse faulting. Similar low-angle reverse faults underlie the ice-proximal sides of Ridge C1 (Appendices, Fig. A3).

RF B also directly underlies the two ice-flow parallel Ridges A2 and A3. The highest reflector is continuous across Ridge A2 but is absent across the crestline of the higher Ridge A3. As with the ice-flow transverse ridges, discontinuities in the reflectors indicate deformation of these horizons. These are best seen in lower reflectors and do not always extend into the highest reflector, particularly on the lower ground to either side of the ridges. An ice-flow parallel radar profile along the long-axis of Ridge A3 reveals onlap and undulations on the ice-proximal side of the ridge, indicating compression in a down-ice direction (Fig. 9). However, there is little displacement transverse to the ice-flow direction, unlike in Ridge A1.

Radar facies A (RF A) underlies RF B at all three sites and consists of relatively short, discontinuous, irregularly dipping reflectors; direction of dip is variable and there is no obvious pattern. At Site A, RF A is visible below RF B under the higher parts of all three ridges, but is not visible under low-lying areas, indicating close association of RF A with ridge formation (Figs. 8 and 9). At Sites C and D, RF A can also be detected under low ground on either side of the ridges. At these sites RF A reflectors are also truncated along the contact with the overlying RF B (Appendices, Figs. A3, A4). At both these sites, a lower reflector appears to pick out a buried surface masked by infill.

### 4.3.2. GPR profiles on mounds: Site B

Local exposures indicate that the surface at this site is immediately underlain by diamicton that is clay-rich compared to Sites A and C. Five radar profile lines were laid out to examine the internal structure of Mounds B1, B2 and B3 (Figs. 10 and 11; Appendices, Fig. A5). Profiles at right angles to each other through Mounds B1 and B2 and the lower ground between the mounds are shown in Fig. 10C and Fig. A5, while parallel profiles through Mound B3 are shown in Fig. 11. As with Site A ridges, the profiles are dominated by strong parallel reflectors sub-parallel to the ground surface (Radar Facies C – RF C); RF C is up to 3 m thick over mounds and up to 5.5 m thick under the low ground between mounds. The reflectors lie parallel to the gently domed surface under the mounds but are irregular and exhibit displacement under hummock side slopes and in the swales between the mounds. In Mound B1 (Fig. 10; Appendices, Fig. A5) this is expressed as distinct troughs or synclines along the southern margin of the mound and in the swale to the south. The troughs/synclines can be traced eastward from radar profile 2 to radar profile 4. These features are not reflected in the surface topography and appear to contain a further infill (Fig. A5). RF C thins eastward and interdigitates with RF A in the lower ground between Mounds B2 and B3 (Figs. 10 and 11).

RF B underlies RF C and consists of short, irregular reflectors. The upper contact of this lithofacies partly reflects the surface topography, with RF C draped over the irregular contact. RF B is best developed to the east of Mound B1 in the lower ground and under Mound B2 (Fig. 10) but continues into the lower areas around these mounds. RF A partly underlies RF C and is visible under Mound B3 (radar profile 5; Figs. 10 and 11), in the low ground between Mounds B2 and B3, and under the south slope of Mound B2. RF A

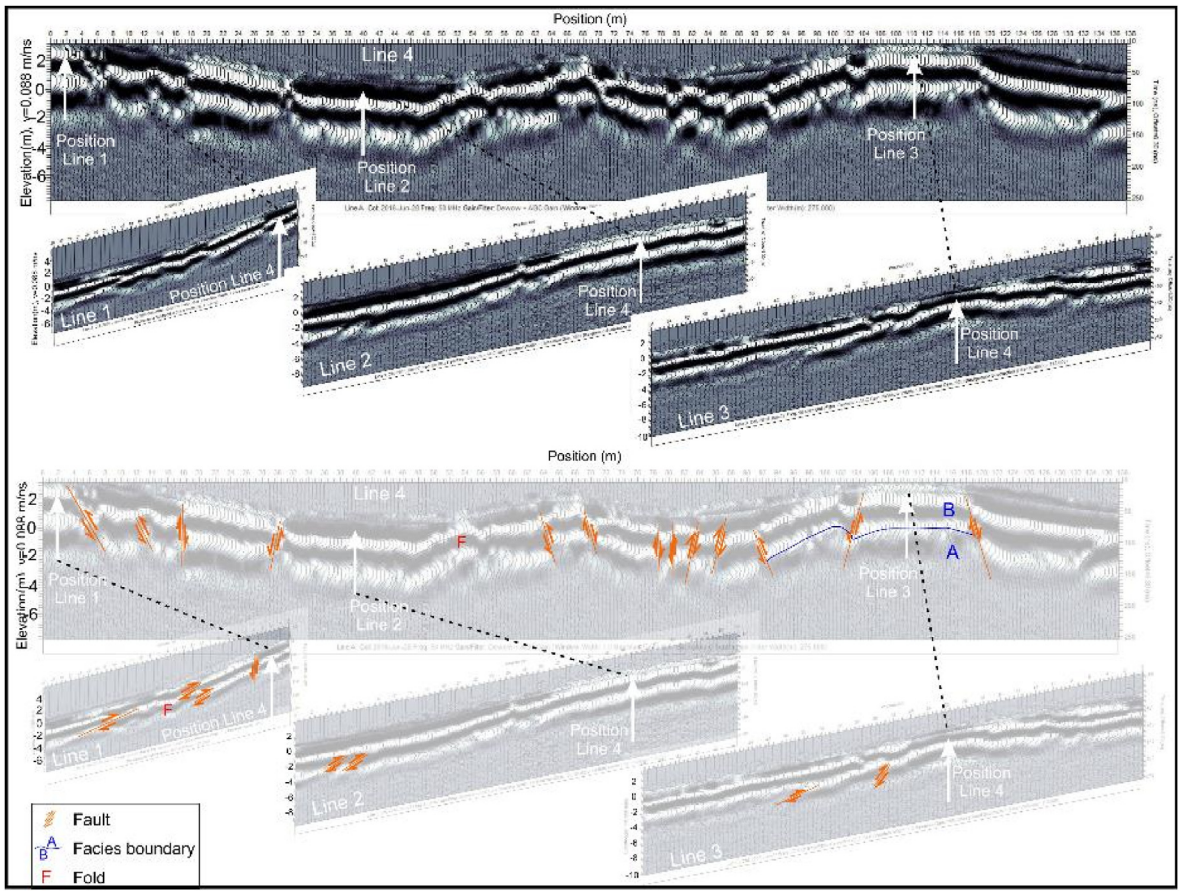


**Fig. 8.** GPR profiles for Ridge A1 with interpretation. Locations of profiles are shown in Fig. 4A.

consists of short sets of parallel reflectors dipping at an angle of <10°; individual sets are up to 20 m long and up to 5 m thick and onlap each other. Reflectors on the southern side of Mound B3 also show evidence of vertical displacement.

A further vertical structure between 20 and 50 m on radar profile 5 is interpreted as a post-glacial feature because it is associated with a cluster of trees that are recorded on 19th century maps. In addition, there is extensive LiDAR DEM evidence of archaeological features, including buildings, field boundary walls and cultivation ridges, which are also recorded on 19th century maps in adjacent fields. It is therefore likely that this feature is related to human activity.

## 5. Interpretation

### 5.1. Geomorphology

#### 5.1.1. Glaciofluvial/glaciolacustrine landforms - eskers and flat-topped mounds

The presence of eskers in the study area indicates a dominantly channelized meltwater drainage system within the ice sheet during their formation. Our mapping indicates that MR are more extensive than previously known. We interpret the chains of smaller mounds at the southeastern ends of the Moate and South Moate MRs as the remnants of englacial or supraglacial channels, deposited on ice and subsequently disturbed during melt. The development of thick topset sequences in at least one delta (flat-topped mound K1; Pellicer et al., 2012) also supports delivery of sediment across the surface of the ice sheet, rather than from a subglacial conduit. The occurrence of these chains of mounds downstream from ice-contact deltas in the South Moate and Moate MRs indicates that the eskers are non-synchronous features, recording meltwater delivery to successive retreating ice margins. The ice margin indicated by flat-topped mound K2 (interpreted here as an ice-contact delta), moraines and the ice-contact delta within the Moate MR is interpreted as a stillstand or readvance ice-marginal position and indicates at least two phases of esker formation in this area. Northwest of this margin a change in morphology in all three MRs indicates a change in meltwater routing within the ice sheet. In the South Moate MR the change north of K2 to multiple small ridges and flat-topped mounds indicates a shift in meltwater delivery from a single, large channel to multiple short channels or conduits, each with a separate discharge. We consider this to indicate a decrease in efficiency in the delivery of meltwater to the margin. On the Moate MR, the change to a continuous, narrow, ridge with one to two crests northwest of the ice-contact delta indicates a possible switch from an en- or supra-glacial channel or conduit to a subglacial to englacial conduit. In contrast, the Horseleap MR, becomes more fragmented north of these moraines, possibly indicating a switch to an englacial or supraglacial conduit/channel.

#### 5.1.2. Hummocky topography

Geomorphological mapping demonstrates that there are one or more preferred orientations to landforms within the hummocky topography. At Sites A, C and D, two dominant alignments are interpreted as follows. Ice flow-parallel alignments consisting of ridge extensions and groups of mounds around Site D have been interpreted previously as buried and fragmented remnants of

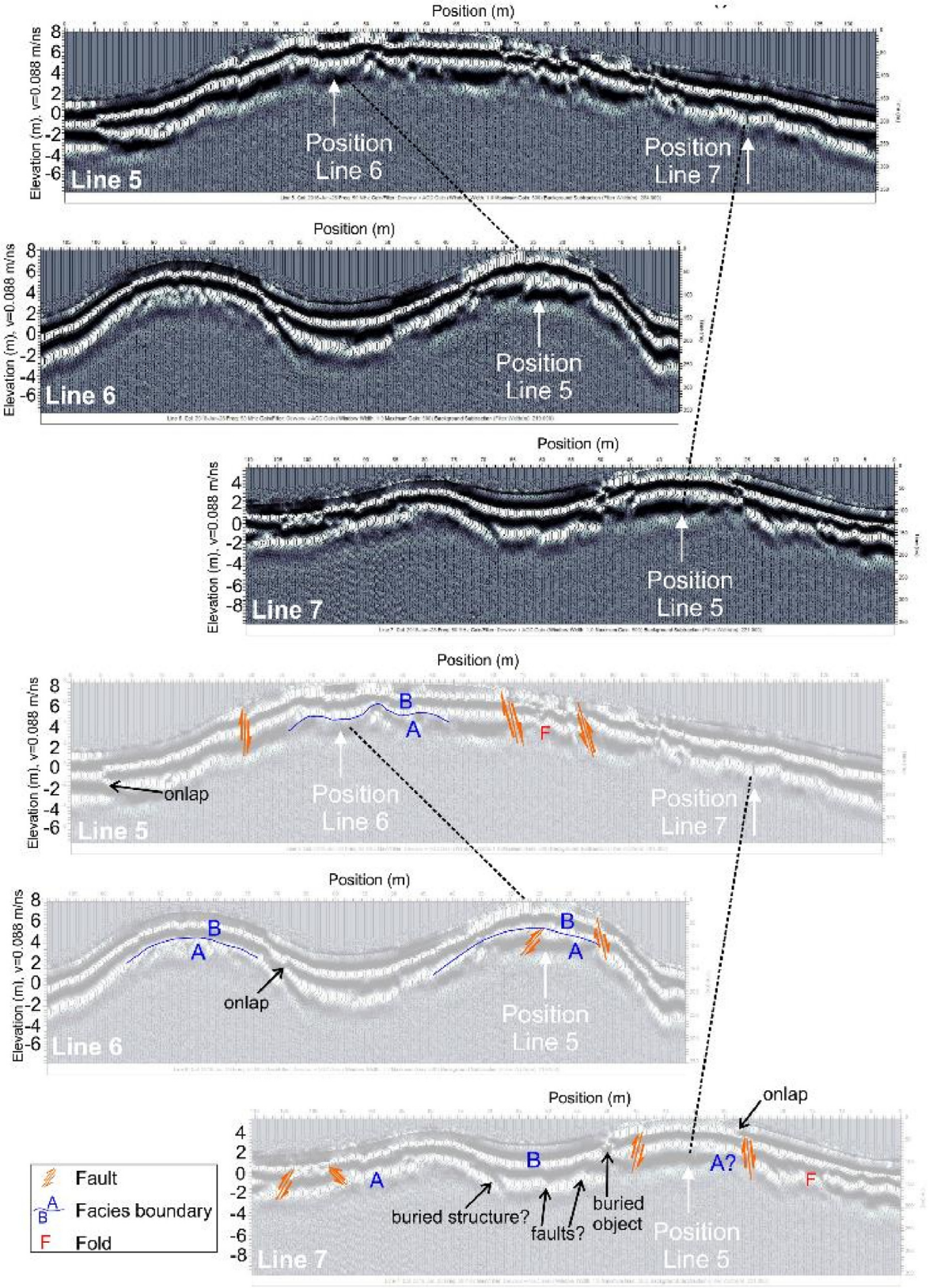


**Fig. 9.** GPR profiles for Ridges A2 and A3, with interpretation. Locations of profiles are shown in Fig. 4A.

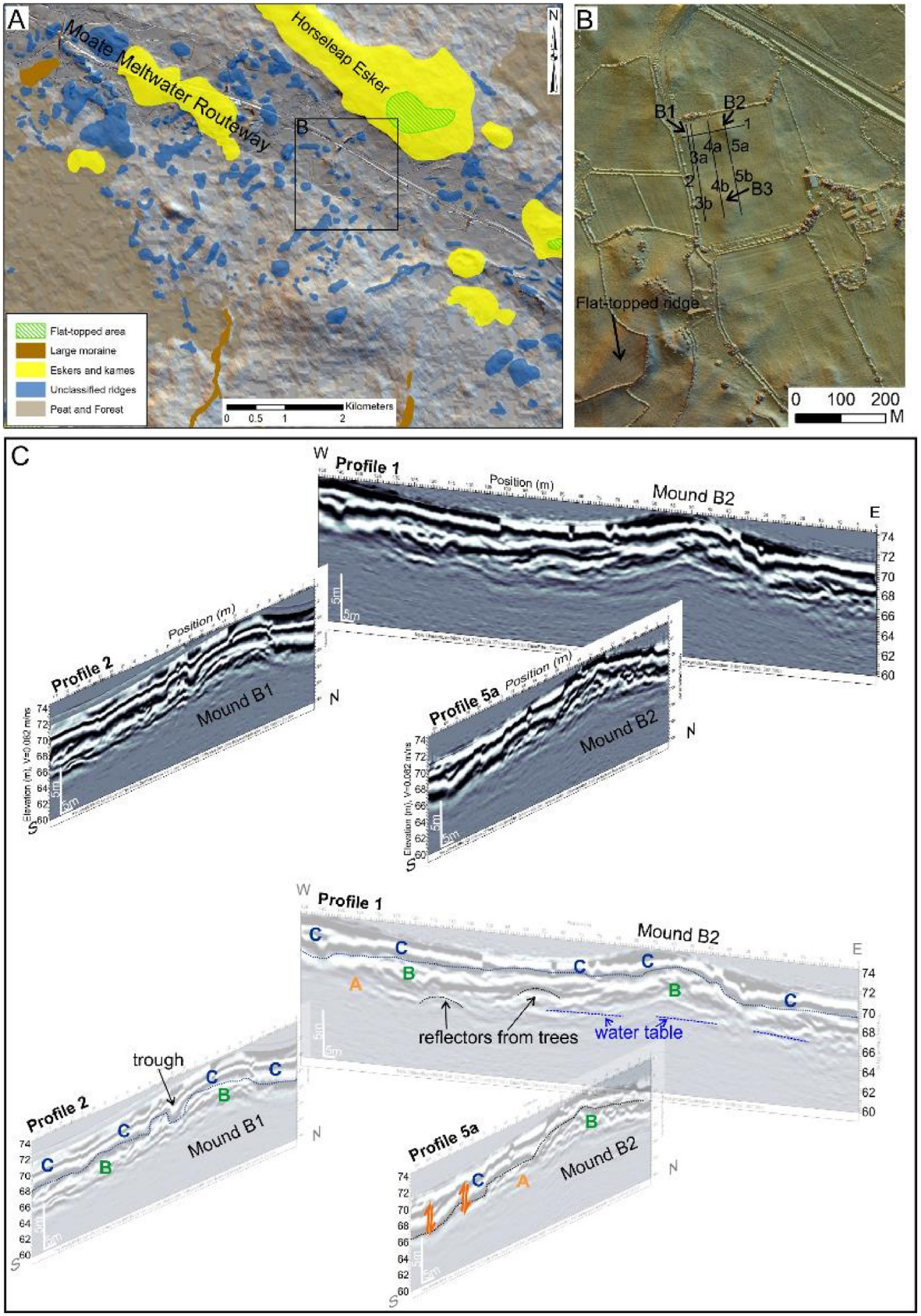


**Fig. 10.** A. Geomorphological map of the area around Site B. Background is a combination of a 1m resolution LiDAR DEM (central part) and 12.5 m resolution radar DEM. B. Close-up of area around Site B, showing the position of GPR profiles. C. GPR profiles and interpretations for Mounds B1 and B2, in Site B.

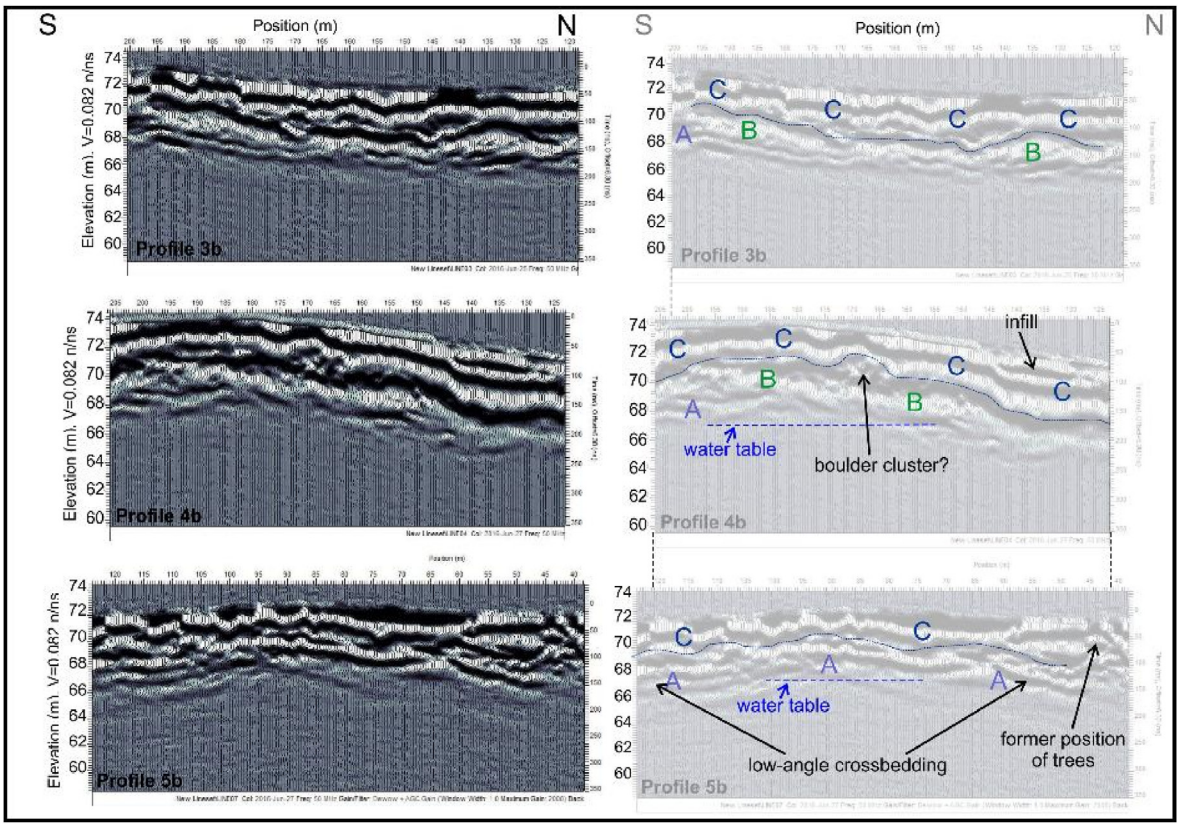


**Fig. 11.** GPR profiles for Mound B3 with interpretation. Location of profile lines is shown in Fig. 10B.

MSGLs (Delaney et al., 2018). At Site C these newly mapped features are also parallel to previously mapped lineations (GSI, 2017; Delaney et al., 2018), and we interpret these also as the remnants of MSGLs. No LiDAR is available for Site A, but since the low ridge extensions have similar dimensions to MSGL fragments at Sites C and D, we also interpret them as MSGL fragments. The fragmented MSGLs are overlain by ice-flow transverse ridges, indicating MSGL formation occurred prior to transverse ridge formation.

At Site A, the streamlined, elongated, ice flow-parallel ridges A2 and A3 are distinct from MSGL fragments and more closely resemble mini-drumlins and drumlinoid features (where asymmetry is poorly developed). In morphology and scale they are similar to small drumlins observed from the beds of modern and Quaternary ice sheets (Smith et al., 2007; King et al., 2009; Dowling et al., 2016; Putniņš and Henriksen, 2017; Hillier et al., 2008; Hart et al., 2018), and we interpret them as such. The mini-drumlins are a similar height to adjacent ridges, and are parallel to streamlining on these ridges, indicating that they are reworked from these ridges.

Small ridges aligned at a high angle or transverse to the inferred ice flow direction are the dominant feature at Sites A, C and D. Equifinality is an issue in identifying the conditions under which these features formed, as similar ridges can form in multiple ways in sub-marginal to ice-marginal settings. Such features have been variably interpreted as crevasse-squeeze ridges (CSRs; Sharp, 1985; Evans and Rea, 1999, 2003; Evans et al., 2016b; Cline et al., 2015; Delaney et al., 2018), as subglacially-formed ribbed moraine (e.g. Stokes and Clark, 2003; Stokes et al., 2008; Dunlop and Clark, 2006; Möller, 2006, 2010; Möller and Dowling, 2015; Peterson et al., 2017; Ojala et al., 2019; Vérité et al., 2021), as controlled moraines formed by meltout of debris-rich bands of ice in a variety of settings (e.g. Evans, 2009; Chandler et al., 2020; Ewertowski and Tomczyk, 2020), as subaerially formed, ice-marginal annual or multi-year terminal moraines, including overridden moraines (e.g. Krüger, 1993, 1995; Matthews et al., 1995; Evans and Twigg, 2002; Evans and Hiemstra, 2005; Chandler et al., 2016, 2020), and as De Geer moraines along the grounding line of a floating ice margin (e.g. Zilliacus, 1989; Lindén and Möller, 2005; Ojala et al., 2015; Bouvier et al., 2015; Ojala, 2016, Appendices, Fig. A6). An additional issue in the Irish Midlands is that after 16,000 years of natural and anthropogenic interaction, ridges have most likely been modified so that crests are subdued and side slopes are at a lower angle than when originally formed. Nevertheless, some geomorphological characteristics of the ridges allow the rejection of certain genetic interpretations.

Firstly, cross-cutting patterns typical of CSRs were not observed at Sites A and C, so this method of formation is not considered further (e.g. Andreasson et al., 2014; Evans et al., 2016b; Delaney et al., 2018). At Site D, some further ridges are imposed obliquely on the main ice-flow transverse ridge set (Fig. 12a in Delaney et al., 2018), but these do not form a rectilinear pattern and may be flutes (see discussion below). Secondly, the ridges described here are much wider than De Geer moraines, and are also more closely spaced (De Geer moraines are generally 9–21 m wide; spacing 20–600m; Ojala et al., 2015; Ojala, 2016). In addition, some of the ridges at Site C lie above the maximum elevation of Palaeolake Riada in that area, indicating that they could not have formed as De Geer moraines at a glaciolacustrine grounding line (Zilliacus, 1989; Bouvier et al., 2015; Ojala et al., 2015; Ojala, 2016; Delaney, 2022).

The arrangement of the ridges is similar to the patterns observed in controlled moraine forming at the margins of modern polythermal glaciers by de-icing of ice cored moraine (Fig. A6 G; e.g. Matthews et al., 1995; Hambrey et al., 1997; Evans, 2009; Krüger et al., 2010a; Hiemstra et al., 2015; Ewertowski and Tomczyk,

2020; Monz et al., 2021). However, they do not particularly resemble fully de-iced Quaternary examples, which are normally dominated by aligned hummocks, rather than ridges, and have well-developed oriented depressions between ridge alignments (e.g. Evans et al., 2014). Ridge asymmetry and the increase in height of ridges where they intersect with an MSGL, along with the evidence for incorporation of material from underlying lineations into the ridges has also been observed during the formation of annual and multi-year ice-marginal moraines (Krüger et al., 2010a). However, while annual ice-marginal ridges observed in front of modern glaciers do occur in groups of multiple ridges like the Brosna basin ridges (e.g. Lukas, 2012; Bradwell et al., 2013; Hiemstra et al., 2015; Chandler et al., 2020), they are much smaller in size and more closely spaced than the Brosna basin examples (modern examples heights <2 m widths <10 m, spacing <30 m). Moraine ridges formed over multiple years at a stationary margin are much closer in scale but have not been observed occurring in groups of multiple ridges (e.g Krüger, 1993; Matthews et al., 1995; Krüger et al., 2010b; Hiemstra et al., 2015). The ridges are also larger than Quaternary examples of annual ice-marginal moraines and lack the sharp crests commonly associated with these features (e.g. Ham and Attig, 2001; Reinardy et al., 2013; Evans et al., 2014; Hiemstra et al., 2015; Chandler et al., 2016, 2020).

The ridges are similar in size and spacing to small ribbed moraine described from the South Swedish Uplands (Supp. Fig. A6 A, E; Möller, 2006, 2010; Möller and Dowling, 2015; Peterson and Johnson, 2017; Peterson et al., 2017; Putniņš and Henriksen, 2017; Ojala et al., 2019; Vérité et al., 2022). The resemblance to small ribbed moraine is also reflected in the shape of ridges at Site A particularly, and to a lesser extent at Sites C and D, including undulating crestlines, inter-ridge spacing close to ridge widths and asymmetric cross-ridge profiles. The partly streamlined surfaces and close association with mini-drumlins at Site A are also features of ribbed moraine (e.g. Möller and Dowling, 2015). The development of flat surfaces on Ridges C1 and C2 reflects water control, and these are interpreted as formed by wave-planation after ice retreat and expansion of proglacial Paleolake Riada (Delaney, 2019, 2022).

Hummocky topography around Site B contains flat-topped features that most likely reflect the control of proglacial lake water levels and are either primary depositional features or, more likely, wave-planed surfaces. The surfaces of these features are between 74 and 80 MOD, close to the lake level in this area during the early stages of Palaeolake Riada (Delaney, 2019, 2022). Overall, the arrangement of mounds (and ridges) in linear groups within hummocky topography reflects structural control by ice, and possibly reflects sub-marginal crevasse patterns. This is discussed further below.

### 5.2. Sediments

We focus on LF 3 sediments in Ridge A1 in the interpretation and discussion below, as these are best exposed and most accessible. Macroscopically, Ridge A1 sediments exhibit a distinct ice-proximal to ice-distal variance, from LF 3 to LF 2. On the ice-proximal side of the ridge in LF 3, the occurrence of partings or planes indicates deposition of the lithofacies as stacked diamictons rather than as a single bed. Such layering in diamictons in ice-flow transverse ridges can develop in a variety of ways in ice-marginal and sub-marginal settings. These include: basal freeze-on, lifting and subsequent deposition by melt-out of rafts of subglacially derived material (Krüger, 1993, 1996; Matthews et al., 1995; Evans and Hiemstra, 2005; Möller, 2010; Hiemstra et al., 2015; Chandler et al., 2016); glaciotectonic thrusting forming imbricate stacked rafts of diamicton, often involving high porewater pressures (e.g. Hambrey et al., 1997; Bennett et al., 1999; Lindén et al., 2008; Putinš and Henriksen, 2017); as stacked glacigenic debris flow deposits (e.g. Lawson, 1982; Evans and Hiemstra, 2005; Lukas et al., 2005; Krüger et al., 2010b; Lukas, 2012); or by a combination of these processes. Distinguishing between these different processes is dependent on identifying an assemblage of features that, when combined, indicate a particular process and environment, rather than specific genetically diagnostic features. An additional issue is that information on microscale structures are confined to one 30 × 20 × 20 $cm^2$ block, so provide information only on a single diamicton layer.

Some formation mechanisms can be discounted immediately. In this case, the absence of pervasive deformation at the macro and microscales, including widespread folding, reverse faulting and smaller deformation features indicates that an origin by glaciotectonic thrusting or bulldozing is unlikely, as sediments deposited in these ways are characterised by widespread deformation (e.g. Hambrey et al., 1997; Lindén et al., 2008; Phillips et al., 2011, 2013).

Other processes require further discussion. The presence of a reasonably well-developed clast fabric combined with alignment of skeleton grains and grain lineaments at the microscale is consistent with shearing during sediment deposition; this could have occurred subglacially due to ice flow (e.g. Hicock, 1990; Benn, 1994; Evans et al., 2007; Evans, 2018), or during laminar flow in a debris flow (e.g. Leigh and Hartley, 1992; Mulder and Alexander, 2001; Lukas et al., 2005) as the eigenvalues and derived isotropy and elongation indices fall within the fabric shape fields for both types of deposition (Benn and Lukas, 2021).

The occurrence of areas of higher fissility, indicating possible zones of higher deformation, could reflect enhanced shearing near the flow base of debris flows (e.g. Lachniet et al., 1999; Mulder and Alexander, 2001; Phillips, 2006; Reinardy and Lukas, 2009), but has also been associated with formation as the B horizon in Icelandic deforming till sequences (e.g. Boulton and Hindmarsh, 1987; Evans et al., 2016b; Evans et al., 2018) and can occur where ridges are formed of stacked slabs of subglacial tractional till (e.g. Krüger, 1993, 1996; Evans and Hiemstra, 2005; Hiemstra et al., 2015; Evans et al., 2018). At the microscale, linear arrangements of otherwise undeformed pores, jigsaw fissures and channels (some of which cut across pre-existing structures) most likely developed post-depositionally along pre-existing lines of weakness such as linear shear structures (e.g. van der Meer and Menzies, 2011; Linch et al., 2012; Linch and van der Meer, 2014; Linch and Dowdeswell, 2016), indicating some shearing throughout the lithofacies.

The presence of microscale intraclasts indicates progressive, though incomplete, incorporation of new material into the sediment, indicating some deformation (e.g. van der Meer, 1993, 1995; Carr, 1999, 2001; Hiemstra, 2001; Evans and Twigg, 2002; Evans and Hiemstra, 2005; Linch et al., 2012; Evans et al., 2012; Menzies, 2012; Linch and van der Meer, 2014; Hiemstra et al., 2015; Linch and Dowdeswell, 2016). Larger inclusions may also be intraclasts of glaciofluvial or glaciolacustrine sediment, incorporated during freeze-on (e.g. Evans and Hiemstra, 2005). The lack of alignment in grain long-axes in the microscale lineaments, and the limited development of skelsepic plasmic fabrics and clast rotation also indicates deformational immaturity (van der Meer, 1993; Menzies, 1998, 2000; Lachniet et al., 1999; 2001; Hiemstra, 2001; Hiemstra and Rijsdijk, 2003; Carr, 2004; Phillips, 2006; van der Meer and Menzies, 2011; Kilfeather et al., 2010; Linch et al., 2012; Linch and van der Meer, 2014; Linch and Dowdeswell, 2016). These lenses of sorted sediment may reflect water sorting during deposition of the diamictons. However typical features of subaqueous debris flows (subaqueous as the ice margin terminated in an ice-contact lake; Pellicer et al., 2012; Delaney, 2022) are absent. For example, internal coarse-tail grading in all or part of the deposit, reflecting differential settling of outsized clasts, laterally continuous lenses of finer sorted sediments (formed by deposition from a

more dilute sediment suspension at the end of the depositional event), or evidence of shallow scouring between bed deposition, also typical of stacked debris flows, are not present (e.g. Lowe, 1976, 1979, 1982; Mulder and Alexander, 2001; Lukas et al., 2005; Reinardy and Lukas, 2009; Talling et al., 2012). In addition, the presence of angular clasts in the lithofacies indicates subglacial incorporation of material with minimal transport, as there is no local source for supraglacial debris (e.g. Evans et al., 2016a, 2018).

High porosity, visible at the microscale, particularly the occurrence of simple packing voids, indicates relatively limited compaction (van der Meer et al., 2010), and may indicate that the stiffness of the diamicton reflects post-depositional cementation rather than subglacial pressure. There is evidence for high water content and high porewater pressure, with laminated structures and multiple domains indicating fluidization/liquefaction of water-sorted sediment (van der Meer, 1993; Menzies, 1998, 2000; Phillips and Auton, 2000; Mahaney et al., 2004; Phillips, 2006; Linch et al., 2012; Linch and van der Meer, 2014; Linch and Dowdeswell, 2016). A clay-filled hydrofracture also indicates high porewater pressure and porewater movement within the sediment, including alignment of clay particles in the direction of porewater movement along the hydrofracture (Phillips, 2006; Linch and Dowdeswell, 2016). High porewater pressures are a feature of debris flows, and the resulting buoyancy is an important transport mechanism within such flows (Mulder and Alexander, 2001; Talling et al., 2012). However, high porewater pressures also occur in submarginal and ice-marginal positions, although this commonly results in more widespread evidence for bed deformation (e.g. Boulton and Hindmarsh, 1987; Boulton, 1996; Evans, 2018; Phillips et al., 2018; Narloch et al., 2020). High porosity and extensive water movement are also associated with deposition by subglacial melt-out (Evans and Hiemstra, 2005; Hiemstra et al., 2015; Larsen et al., 2016), although the preservation of melt-out till on a slope seems unlikely (Evans, 2018).

Overall, while LF 3 contains evidence for subglacial transport at both the macro- and micro-scale, this is limited compared to observations of many modern and Quaternary subglacial traction tills. Equally, evidence for gravity and water sorting is ambiguous (Reinardy and Lukas, 2009; Lukas, 2012; Evans, 2018). Similar inconsistencies between microscale and macroscale characteristics of diamictons have been observed in submarginally deposited tills previously (e.g. Evans and Hiemstra, 2005; Hiemstra et al., 2015; Evans et al., 2016a; Evans et al., 2018) and has been suggested to reflect the considerable spatial and temporal variability in shear stress, sediment strength, porewater pressure and connectivity in subglacial sediments that leads to vertical and lateral variation in deformation (Evans et al., 2016a, 2018; Phillips et al., 2018). The most likely model for the formation of LF 3 is by a combination of processes, including basal freeze-on, slab emplacement and melt-out of subglacial sediments, and subsequent reworking of subglacially derived sediments in sediment gravity flows as de-icing occurred.

In comparison to LF 3, LF 2 contains clear evidence for water sorting, including stratification and distinct lenses of coarse and fine sand. The presence of these more continuous layers of fine material is consistent with wash horizons between sediment gravity flows, such as debris flows, rather than direct glacial deposition (Lawson, 1982; Reinardy and Lukas, 2009; Lukas, 2012; Evans, 2018). We interpret this lithofacies as composed predominantly of sediment gravity flow deposits that form the core and ice-distal side of the ridge. Due to limited evidence the origin of LF 1 remains ambiguous. However, the occurrence of a diamicton below the level of the surrounding land surface indicates a prior phase of glacigenic deposition prior to ridge formation.

Sediment exposures in the area around Site D indicate a likely similar origin for ridges. However, the presence of a blocky diamicton with evidence of clast crushing around Site C indicates high stresses and possible overriding by ice.

### 5.3. GPR

Several structural features are identifiable within all GPR profiles of the ridges. Firstly, all GPR profiles indicate that the ridges and mounds examined are immediately underlain by similar sediment (RF B at Sites A, C and D, RF C at Site B). This is expressed as strong, semi-continuous, parallel reflectors that approximately mirror the surface topography. We interpret this radar facies as diamicton, which is confirmed by sedimentary exposures in the ridges, and the interpretation of similar radar facies in glacial and paraglacial landforms elsewhere (e.g. Sadura et al., 2006; Stokes et al., 2008). We do not consider these widely spaced reflectors to indicate bedding (i.e. they are not consistent with the stratigraphy exposed in Ridge A1); rather they are likely to reflect soil profile characteristics and groundwater-controlled changes in hydraulic conductivity (groundwater depths typically 2–6 m).

Faulting is visible in radar profiles at all sites, consistent with similar structural features in glacial and paraglacial landforms elsewhere (e.g. Jakobsen and Overgaard, 2002; Sadura et al., 2006; Florentine et al., 2017; Andersen and Jakobsen, 2018). The pattern of faulting varies between ridge and mound types and is discussed further below.

For ice-flow transverse ridges at Sites A, C and D, RF B overlies a second facies (RF A), which represents more stratified sediment. RF A is better represented at Sites C and D, where bedding structures are truncated, and we interpret this as evidence for overriding of previously deposited glaciofluvial or sediment gravity flow deposits, indicating multi-phase formation of ridges at these sites. At Site C, the remnant of an MSGL can also be detected underlying RF B.

Displacements of reflectors within RF B on ice flow-parallel profiles at all three sites indicate that low-angle reverse faults occur on the ice-proximal side of these transverse ridges. At Site A, these reverse faults have a similar dip to planes identified in sediment LF 3, confirming that they are structural features, and we interpret these as thrust faults or shear planes, indicating displacement of material by ice movement. The ice flow-transverse profile along Ridge A1 crestline also indicate displacements around high points, interpreted here as normal faults and high-angle reverse faults. Both types of faulting are associated with melting of discrete buried ice masses (e.g. McDonald and Shilts, 1975) and support an interpretation as most likely due to post-depositional settling as buried ice in the ridge melted. This pattern is also observed on the ice-distal side of Ridge C1.

In the larger of the two ice flow-parallel ridges at Site A (Ridge A3) displacements under the ice-proximal side of the ridge also indicate low-angle reverse faulting, with bending of the associated reflectors towards the crest of the ridge interpreted here as shallow folding. A further reflector under the crest of Ridge A2 may also be a fault, as it is associated with displacement of the overlying reflector. As with ice flow-transverse ridges, the faulting and folding pattern in the ice flow-parallel ridges indicates the application of a directional force from the WSW, consistent with ice push along the ice-proximal side of both ridges, and the features are interpreted as glaciotectonic in origin. In all profiles, the thickening of reflectors into swales is a feature and is interpreted as post-glacial colluvial reworking of these sediments.

Radar profiles across mounds at Site B indicate a somewhat different facies geometry. RF C indicates a cover of diamicton across this site, but facies thickness is more variable than at other sites and thins laterally, so the underlying RF B is more clearly visible on the

profiles. The distinct sets of shorter parallel reflectors in this radar facies are interpreted as co-sets of low-angle cross-bedding, consistent with glaciofluvial deposition, and indicating aggradation in more than one direction. The GPR profiles show some open folds and normal faults in RF C, indicating some vertical displacement occurred at the mound margins, but we do not consider there to be evidence of compressional deformation. We interpret this displacement as most likely caused by post-depositional gravitational settling, due to the melting of buried ice. The depression traceable through radar profiles 2–4 may be a fold, a faulted block or graben, or a small meltwater channel excavated on the surface and subsequently infilled.

Overall, the mounds are interpreted as supra-glacial to ice-marginal features initially deposited partly on stagnant ice. The diamicton on the western side of the site may be supraglacial meltout diamicton, or glaciofluvial and glaciolacustrine sediments reworked by debris flows.

## 6. Discussion

Both geomorphologic evidence and internal composition and structure indicate that areas of hummocky topography comprise a composite of landforms, reflecting multiple phases of glacial activity.

### 6.1. Formation of MSGLs

LiDAR DEMs and GPR profiles show that the oldest landforms are MSGLs, as they underlie other glacigenic landforms around Sites A, C and D. MSGLs are considered to form under wet-based ice due to sediment erosion, transfer and deposition in areas with a dilatant, deforming bed (e.g. King et al., 2009; Smith and Murray, 2009; Ó Cofaigh et al., 2013; Stokes, 2018; Schlegel et al., 2022). Their occurrence in the central Irish Midlands is significant, as they are associated with accelerated ice flow in ice streams and surging glaciers (Clark, 1993; Stokes and Clark, 2002; Andreasson et al., 2014; Flink et al., 2017; Ó Cofaigh et al., 2013; Stokes, 2018). MSGLs have previously been identified in other parts of the Brosna basin and at one site are associated with CSRs and interpreted as indicating episodic surging of the ice sheet (Delaney et al., 2018; Delaney, 2022). Their occurrence at Sites A, C and D indicates that at least one phase of accelerated ice flow occurred prior to the formation of hummocky topography and glaciofluvial/glaciolacustrine landforms in the basin.

### 6.2. Hummocky topography formation

MSGLs are overlain by, and have been partly incorporated into, low, short ridges deposited at a high angle or transverse to ice flow. Fragmentation of MSGLs and the presence of low-angle thrust faults identified on the ice-proximal side of ridges and immediately up-ice of ridges, combined with evidence of shear planes in the sediments exposed in Ridge A1, indicates that ridge formation involved a change from ductile to brittle deformation and thus a change in bed rheology. This resulted in recoupling of the base of the ice sheet with the underlying sediments and a decollement in the basal debris zone, as indicated by faulting. Such a change in bed conditions has been observed or modelled in both subglacial and sub-marginal areas, related to a change in either thermal or hydrological regimes, or both. Reorganisation of the subglacial meltwater regime from a distributed to a linked cavity or a channelized system, has been suggested to result in a reduction in lubrication and ice velocity in glaciers and ice sheets and an increase in longitudinal compressive stresses (e.g. Patterson, 1997; Bingham et al., 2003; Sundal et al., 2011; Tedstone et al., 2015; Vérité et al., 2021). Alternatively, a similar effect can be generated by a thermal transition from an unfrozen to a frozen bed, resulting in freeze-on of sediment (e.g. Christoffersen and Tulaczyk, 2003a, b; Monz et al., 2021). The angular nature of clasts at Ridge A1 indicates localised input of sediment and short subglacial transport distances (e.g. Evans et al., 2016a).

The combined morphological and sedimentological characteristics of the ridges suggest that they were formed by displacement and stacking of till slabs, followed by melt-out and reworking of materials by sediment gravity flows, giving rise to an asymmetric cross-profile in many ridges. The extensive evidence of enhanced porewater movement and sediment flow, with evidence of post-depositional vertical displacement of sediment, indicates a high ice content in the sediment during initial deposition. Similar combinations of sedimentological and structural features have been observed in ridges at modern Arctic temperate and polythermal glaciers (e.g. Krüger, 1993, 1996; Matthews et al., 1995; Bennett et al., 2010; Evans and Hiemstra, 2005; Bennett and Evans, 2012; Hiemstra et al., 2015; Tonkin et al., 2017), and in Quaternary small ribbed moraine formed in sub-marginal settings (Möller, 2010; Möller and Dowling, 2015). In modern temperate glacier ice-marginal settings, such ridges form by incremental growth due to incorporation of basal sediment by seasonal refreezing of the glacier to its bed, followed by winter readvance and release of material associated with formation of a seasonal or multi-year frozen toe as the ice thins toward the margin (e.g. Evans and Hiemstra, 2005; Hiemstra et al., 2015). This reflects the presence of a thermal boundary at least seasonally.

An alternative model for ridge formation observed at both modern temperate and polythermal ice margins occurs where debris-rich basal ice moves upwards to form englacial and supraglacial debris bands in a compressional flow zone around the ice margin. This was previously thought to involve thrusting and extensive glaciotectonization of sediment, not observed in the sediments at Ridge A1 (e.g. Hambrey et al., 1997; Bennett et al., 1999). However, recent observations at polythermal glaciers indicate that thrusting and shearing plays a limited role and instead sediment incorporation and upward movement can happen by refreezing of sediments along pre-existing fractures at the down-ice transition from warm-to cold-based ice near the margin (Evans and Hiemstra, 2005; Hiemstra et al., 2015; Monz et al., 2021). Incorporation of sediment occurs in areas of longitudinally compressive ice flow, reflecting either topography or changes in ice characteristics (e.g. Hambrey et al., 1997; Swift et al., 2006; Monz et al., 2021). Topographic control is unlikely here, as the ridges all occur on flat or very low angle slopes; this also discounts the incorporation of sediment due to refreezing of supercooled water at the downstream end of an overdeepening, another mechanism of sediment entrainment (e.g. Lawson et al., 1998; Speddings and Evans, 2002; Swift et al., 2006; Bennett et al., 2010; Cook et al., 2010; Bennett and Evans, 2012; Swift et al., 2018). Instead, compression could have occurred due to changes in ice thickness, hydrological or thermal conditions, for example if there is a transition from warm- to cold-based ice toward the glacier margin (e.g. Krüger, 1993; Hambrey et al., 1997; Glasser et al., 2003; Monz et al., 2021), or in association with readvance over a pre-existing body of sediment and or ice, where fracturing and crevasse-filling and/or thrusting occurs (e.g. Bennett et al., 1999; Sletten et al., 2001; Evans et al., 2012). This scenario has also been proposed to generate small ribbed moraine in a zone close to the ice margin (Lindén et al., 2008; Möller, 2010; Möller and Dowling, 2015; Vérité et al., 2021, 2022).

At modern polythermal ice margins, sediments moved to englacial or supraglacial positions in this way are subject to reworking when underlying ice melts and it has been suggested that

ultimately any linearity will disappear as melting continues, which can take hundreds/thousands of years (e.g. Tonkin et al., 2016; Ewertowski and Tomczyk, 2020). Where the thrust or fracture plane is at a low angle, as they usually are, debris can be spread over a wide area so no significant ridge is formed (Lukas et al., 2005; Evans, 2009). However, modern observations are, of necessity, confined to the supraglacial and ice-marginal areas of glaciers, so it is possible that ridges may form and be preserved in the sub-marginal zone, at the upstream end of a zone of compression (discussed further below). In any case, for ridges to form in this manner a very high sediment content is necessary toward the base of the fracture fill and, possibly, removal of material from higher in the fill by sediment gravity flow as the resulting flow deposits would end up beside the original ridge and thus mask it (e.g >40% sediment; Glasser et al., 2003; Evans, 2009; Ewertowski and Tomczyk, 2020). Another issue with this interpretation of the ridges as controlled moraine is the absence of obvious kettles or closed depressions typically formed by meltout of buried ice (e.g. Dyke and Evans, 2003; Evans, 2009, 2010; Evans et al., 2014).

One aspect of these ridges not observed at modern ice margins is the reshaping, resulting ultimately in mini-drumlin formation at Site A. Mini-drumlins such as these are suggested to form rapidly (<30 years) by a combination of erosion of a pre-existing obstacle or sticky spot (in this case a ridge) by a deforming till layer, followed by deposition of a subglacial traction till carapace at the end of the erosional event (Jónsson et al., 2016; Dowling et al., 2016; Hart et al., 2018). The occurrence of these features along the southern margin of Site A indicates further ice flow occurred after ridge formation, as a result of either overriding by a readvance or reactivation of wet-based flow. However, readvance over the entire group of ridges seems unlikely, as the ridges are relatively steep sided compared to modern overridden ridges (e.g. Guðmundsson and Evans, 2022).

The ridges at Site A in particular bear a resemblance to minor ribbed moraine described from Sweden and Finland and dating from the end of the Last Glacial Termination (Lindén et al., 2008; Möller, 2010; Möller and Dowling, 2015; Peterson et al., 2017; Ojala et al., 2019; Vérité et al., 2022). In the south Swedish Uplands a 20–40 km wide belt formed of combined ribbed moraine and hummocky moraine and punctuated by meltwater corridors extends transverse to the reconstructed ice flow direction and is suggested to have formed in the sub-marginal zone (Lindén et al., 2008; Möller, 2010; Möller and Dowling, 2015; Peterson et al., 2017; Ojala et al., 2019; Vérité et al., 2022). These Scandinavian ridges are also partly streamlined transverse to their long axis and exhibit similar ice-proximal to ice-distal variation in their internal structure, i.e. proximal sediments are diamictons displaying similar evidence for meltwater release and porewater movement, while distal sediments are crudely stratified (Möller, 2010; Möller and Dowling, 2015). Consequently, we suggest that Site A ridges are a further example of these minor ribbed moraine. However, no modern analogues that can be related to glacier characteristics have been identified for these features.

The truncation of previously deposited, stratified sediments at Sites C and D may also indicate post-depositional overrunning by ice at these sites. At Site D, overprinting of ice-flow transverse ridges with further small ridges aligned oblique to the overall ice flow direction has also been observed (Delaney et al., 2018). These have been suggested to be CSRs. However, interpretation of such narrow, low features (5–10 m wide, <50 m long, 0.5 m high) is difficult, even with high resolution DEMs, as post-depositional modification due to natural and agricultural activities have softened the crestlines and basal break of slopes. The obliquely-aligned ridges at Site D are relatively straight and may actually be poorly preserved flutes. In any case, whether these are CSRs or flutes, the ridges indicate a further episode of submarginal activity. At Site C, no evidence for overriding was observed, and the GPR evidence for diamicton deposition does not provide any information about the nature of the sediment.

The mounds at Site B indicate supraglacial deposition of both sorted and unsorted sediments; in this case, sediments may have been deposited directly on the ice sheet surface from supraglacial streams, deposited in englacial conduits, or moved upward from a subglacial position and reworked; all these pathways have been observed at modern temperate and polythermal glaciers (see below; e.g. Bennett and Evans, 2012; Storrar et al., 2015, 2020; Evans et al., 2022).

Overall, the evidence for the origin of the Brosna basin ridges is ambiguous. At Site C, the ability to link ridges laterally and the absence of evidence of subsequent remoulding by ice is more consistent with formation as ice-marginal moraines. Ridges at Site D are also traceable laterally, although there is evidence of further remoulding, and they may have been overridden. However, at Site A, the absence of clear ice-marginal alignment of ridges, together with the evidence for subsequent streamlining of the ridges is more consistent with a submarginal origin as ribbed moraine.

The possibility of a different origin for the ridges at Site A versus Site C also raises the possibility that they were not formed at the same time, as they lie on either side of a well-defined stillstand or readvance margin position.

### 6.3. Formation of glaciofluvial-glaciolacustrine landforms

The three parallel, channelised meltwater drainage systems that developed within the ice sheet along the northern margin of the Brosna basin maintained a relatively stable position through two phases of formation, separated by an ice-marginal stillstand or readvance. The meltwater routeways are more closely spaced (<5 km apart) than is typical of Quaternary meltwater routeways elsewhere, where spacings between 8 and 15 km are typical (e.g. Boulton et al., 2009; Storrar et al., 2014; Lewington et al., 2020) and this indicates considerable meltwater discharge during ice retreat in this area (Storrar et al., 2014). Changes in morphology also indicate a reorganisation of the meltwater drainage system following the ice margin stillstand/readvance. Prior to this, ice-contact glaciofluvial deposition took place in en- or supra-glacial conduits or channels, feeding to large deltas at the ice margin. Channelised surface and near-surface meltwater movement has been observed at both temperate and polythermal modern ice margins. They may be fed directly by supraglacial meltwater (e.g. Fountain et al., 2005; Gulley et al., 2009; Irvine-Fynn et al., 2011), or evolve from a sub- or en-glacial conduit system. The latter can happen through down-wasting of ice and collapse of en/subglacial conduit roofs, associated with glacier karst development, although not necessarily with stagnant ice (e.g. Price, 1969; Bennett et al., 2010; Irvine-Fynn et al., 2011; Bennett and Evans, 2012). Alternatively, upward movement of pressurized subglacial meltwater can transport sediment onto the surface (e.g. Gustavson and Boothroyd, 1987; Gulley et al., 2009; Irvine-Fynn et al., 2011; Evans et al., 2012; Storrar et al., 2020; Karušs et al., 2021; Evans et al., 2022). In many cases this is associated with non-temperate ice, for example, in the ice-marginal zone of a polythermal glacier where pressurized water moves upward in the temperate-to-cold ice transition zone, often exploiting weaknesses in the ice, such as fractures (e.g. Skidmore and Sharp, 1999; Irvine-Fynn et al., 2011; Evans et al., 2012, 2022; Karušs et al., 2021). These en- to supra-glacial channels can reach a considerable size and complexity (up to 120 m wide; Karušs et al., 2021). At temperate ice margins, upward movement of meltwater is often associated with subglacial outburst floods, either due to release of subglacial lake waters (e.g.

Roberts et al., 2000; Russell et al., 2006) or at the end of a surge event (e.g. Evans et al., 2012; Storrar et al., 2015, 2020; Evans et al., 2022). Formation due to a post-surge outburst flood has been suggested for the Birr Esker, due to the fan-shaped nature of the multi-ridged section and the development a partly rectilinear ridge arrangement (Delaney et al., 2018; Storrar et al., 2020; Evans et al., 2022). However, this geometric pattern is not present in the narrower ridge complexes in eskers and mound groupings around Sites A, B and C, and the development of en- and supra-glacial channels indicates either the development of glacier karst on a temperate glacier (e.g. Price, 1969) or possibly the presence of basal cold ice in the ice marginal zone during esker formation, preventing downward drainage of water. Evidence of hummocky topography formed by de-icing at Site B supports the former interpretation but does not preclude the latter.

Northwest of the stillstand/readvance margin associated with ice-contact delta K2, a large subglacial conduit fill leading to an ice-marginal delta forms the Moate MR, while both the South Moate and Horseleap MRs become smaller and more fragmented. This change most likely reflects the capture of drainage areas by the Moate MR from the two adjacent MRs as the subglacial conduit enlarged (Shreve, 1972) so that the Moate MR became the main drainage route, with localised drainage only in the South Moate MR. This reconfiguration may be related to temporary stabilisation of the ice margin during construction of ice contact delta K2 and the delta at the esker termination in the Moate MR.

### 6.4. Timing of formation and ice sheet characteristics

Establishing the relative age of the complex of features within the Brosna basin is difficult, as direct stratigraphic information is not always available. MSGLs underlie all other features and there may be a significant age gap between their formation and subsequent events. Around Site A, ridges within hummocky topography are overlain by glaciofluvial features associated with the K2 delta margin, indicating that these ridges formed before the second phase of esker formation and also likely predate ridge formation at Site C, as a major ice margin lies between these two sites. However, the continuity of the MRs in the northern Brosna basin indicates that features on either side of these margins were likely formed in relation to the same overall ice margin configuration and within a relatively short period of time. Tracing of ice marginal positions across the Brosna basin indicates that hummocky topography and eskers around Site D are of similar age. These features can be considered collectively as a glacial landsystem.

Comparison with modern landsystem analogues does not reveal an obvious counterpart to the Brosna basin landsystem as a whole. During the initial stages of retreat, the controlled moraine formed at Site B and the extensive englacial and supraglacial glaciofluvial deposition is comparable to landform assemblages described from both active temperate glaciers with a high surface debris content, and polythermal glacier systems characterised by a cold ice zone at the ice margin, but with interior warm-based ice, including surging polythermal glaciers (Dyke and Evans, 2003; Glasser and Hambrey, 2003; Evans et al., 2012). However, while groups of parallel ridges can occur in both active temperate and polythermal glacial landsytems, as either ice-marginal moraines or controlled moraine, morphological evidence is not consistent with either interpretation, either due to differences in scale and lateral continuity, or due to the absence of features such as kettles and evidence for partial reshaping by overriding ice.

An alternative possibility for generation of the ridges described above is provided by recent analogue modelling of ice streams by Vérité et al. (2021), which generated a belt of small ribbed moraine in the submarginal zone, aligned parallel to the margin of the modelled ice stream lobe. The model suggests that the ribbed moraine formed due to ice flow deceleration caused by the development of a channelised drainage system toward the ice stream margin. The arrangement of the modelled sub-marginal ridges in an ice-flow transverse belt is also seen in ribbed moraine of the South Swedish uplands described above, and recent mapping suggests that the ridge groups at Sites A and C form part of a similar belt of ridges that extends southward across the Brosna basin to the area around site D. In all three cases, the ice-flow transverse belt of ridges is punctuated by large meltwater corridors or routeways indicating meltwater channelisation (Delaney, 2022). One possibility is that the zone of ridges in the Brosna basin marks the deceleration of a major surging event as suggested by McCabe (2008) and indicated by the occurrence of MSGLs up-ice from and underlying the ridges. However, further study of the hummocky topography, including dating to establish an event chronology, is necessary to test this hypothesis especially as evidence from further east indicates that more than one episode of accelerated ice flow occurred in the Brosna basin (Delaney et al., 2018). Finally, while ridges at Site A resemble minor ribbed moraine, ridges at Sites C and D or more likely to have formed ice-marginally, indicating a complex origin for this hummocky moraine belt.

## 7. Conclusions

Integration of high resolution geomorphological, sedimentological and geophysical evidence shows that hummocky topography within the Brosna basin is formed of a complex continuum of landforms that reflect evolving subglacial rheology during ice sheet retreat. Fragmented MSGLs indicate a previously unknown phase of accelerated (streaming or surging) ice flow southeastward along the northern margin of the basin, indicating a wet-based ice sheet. A subsequent shift in bed thermal and/or hydrological conditions led to partial recoupling of the ice to its bed in patches, followed by detachment of sediment rafts from the MSGLs and construction of sub-marginal ribbed moraine immediately down-ice, associated with longitudinal compression toward the ice sheet margin. This was most likely due to ice flow deceleration toward the ice margin due to dewatering and/or a thermal transition from warm to cold ice, and may have been related to a surge. This resulted in redirection of meltwater from the bed and transport of sediment upward into englacial and supraglacial conduits and channels and onto the ice surface, subsequently generating further hummocky topography composed of aligned mounds due to meltout of buried ice. Subsequent retreat of the ice margin was followed by reorganisation of this en-/supra-glacial drainage system to a more efficient subglacial conduit system. Further small ridges within hummocky topography may have formed ice-marginally during further retreat or may represent up-ice migration of a zone of longitudinal compressive strain. The landforms were generated at either an active temperate or a polythermal ice margin.

Our results indicate that the zone of hummocky topography within the Brosna basin has a complex origin and formed in a variety of ways in the sub-marginal to marginal zone. While modern analogues cast some light on the mechanisms involved in formation of hummocky topography, it is possible that no appropriate analogues have been identified for minor ribbed moraine that developed in the sub-marginal zone of the ice sheet. Further characterisation of the many types of small ridges generated by glacial systems is needed to evaluate this possibility. Our work demonstrates the usefulness of hummocky topography in identifying changes in ice sheet bed thermal/hydrological characteristics during deglaciation and the importance of combining multiple evidence strands in reconstructing the processes involved in glacial landform construction.

## Author contributions

Delaney, C.: conceptualization, funding, methodology, data acquisition, visualization, writing and editing. Adamson, K.: conceptualization, funding, methodology, acquisition and analysis of ground-penetrating radar data, writing and editing. Linch, L.: methodology, acquisition and analysis of sedimentological data, visualization, writing and editing. Davis, S.: methodology, processing and analysis of LiDAR data, visualization, editing. McCarron, S.: conceptualization, data acquisition and analysis, editing.

## Declaration of competing interest

The authors declare that they have no known competing financial interests or personal relationships that could have appeared to influence the work reported in this paper.

## Data availability

Data will be made available on request.

## Acknowledgements

Fieldwork for this research was undertaken with the support of a research grant from the British Society for Geomorphology. We thank Dr. Adrian Palmer, Royal Holloway, University of London, for assistance with thin section preparation. We thank Prof. David J.A. Evans, Dr. Sven Lukas and one anonymous reviewer for their constructive and detailed reviews, that greatly improved the paper.

## Appendix A. Supplementary data

Supplementary data to this article can be found online at https://doi.org/10.1016/j.quascirev.2023.108041.

## References

Allmendinger, R.W., Cardozo, N., Fisher, D., 2013. Structural Geology Algorithms: Vectors and Tensors. Cambridge University Press, U.K., p. 289
Andersen, C.S., Jakobsen, P.R., 2018. Sedimentological and glaciotectonic interpretation of georadar data from the margin of the Vig ice-push ridge, NW Sjælland, Denmark. GEUS Bulletin 41, 25–28.
Andreasson, K., Winsborrow, C.M., Bjarnadóttir, L.R., Rüther, D.C., 2014. Ice stream retreat dynamics inferred from an assemblage of landforms in the northern Barents Sea. Quat. Sci. Rev. 92, 246–257.
ASF DAAC, 2007. ALOS PALSAR radiometric terrain corrected high resolution [Online] Available at: https://asf.alaska.edu/data-sets/derived-data-sets/alos-palsar-rtc/alos-palsar-radiometric-terrain-correction/ [Accessed October 2018].
Attig, J.W., Clayton, L., 1993. Stratigraphy and origin of an area of hummocky glacial topography, northern Wisconsin, U.S.A. Quat. Int. 18, 61–67.
Benn, D.I., 1992. The genesis and significance of 'hummocky moraine': evidence from the Isle of Skye, Scotland. Quat. Sci. Rev. 11 (7–8), 781–799.
Benn, D.I., 1994. Fabric shape and the interpretation of sedimentary fabric data. J. Sediment. Res. 64, 910–915.
Benn, D.I., Evans, D.J.A., 2010. Glaciers and Glaciation, second ed. Hodder Education, London.
Benn, D.I., Lukas, S., 2006. Younger Dryas glacial landsystems in North West Scotland: an assessment of modern analogues and palaeoclimatic implications. Quat. Sci. Rev. 25, 2390–2408.
Benn, D.I., Lukas, S., 2021. Chapter 5: Macrofabric. In: Evans, D.J.A., Benn, D.I. (Eds.), A Practical Guide to the Study of Glacial Sediments. Quaternary Research Association, London, pp. 125–154.
Bennett, G.L., Evans, D.J.A., 2012. Glacier retreat and landform production on an overdeepened glacier foreland: the debris-charged glacial landsystem at Kviárjökull, Iceland. Earth Surf. Process. Landforms 37, 1684, 1602.
Bennett, M.R., Hambrey, M.J., Huddart, D., Ghienne, J.F., 1996. The formation of a geometrical ridge network by the surge-type glacier Kongsvegen, Svalbard. J. Quat. Sci. 11 (6), 437–449.
Bennett, M.R., Hambrey, M.J., Huddart, D., et al., 1999. The landform and sediment assemblage produced by a tidewater glacier surge in Kongsfjorden, Svalbard. Quat. Sci. Rev. 18, 1213–1246.
Bennett, G.L., Evans, D.J.A., Carbonneau, P., Twigg, D.R., 2010. Evolution of a debris-charged glacier landsystem, Kvíaírjökull, Iceland. J. Maps 6 (1), 40–67.
Bingham, R.G., Nienow, P.W., Sharp, M.J., 2003. Intra-annual and intra-seasonal flow dynamics of a High-Arctic polythermal valley glacier. Ann. Glaciol. 37, 181–188.
Boone, S.J., Eyles, N., 2001. Geotechnical model for great plains hummocky moraine formed by till deformation below stagnant ice. Geomorphology 38, 109–124.
Boulton, G.S., 1996. The origin of till sequences by subglacial sediment deformation beneath mid-latitude ice sheets. Ann. Glaciol. 22, 75–84.
Boulton, G.S., Hindmarsh, R.C.A., 1987. Sediment deformation beneath glaciers: rheology and geological consequences. J. Geophys. Res. Solid Earth 92 (B9), 9059–9082.
Boulton, G.S., Hagdorn, M., Maillot, P.B., Zatsepin, S., 2009. Drainage beneath ice sheets: groundwater-channel coupling, and the origin of esker systems from former ice sheets. Quat. Sci. Rev. 28, 621–638.
Bouvier, V., Johnson, M.D., Påsse, T., 2015. Distribution, genesis and annual origin of De Geer moraines in Sweden: insights revealed by LiDAR. GFF 137 (4), 319–333.
Boyes, B.M., Linch, L.D., Pearce, D.M., et al., 2021a. The Kola Peninsula and Russian Lapland: A review of Late Weichselian glaciation. Quat. Sci. Rev. 267, 107087.
Boyes, B.M., Pearce, D.M., Linch, L.D., 2021b. Glacial geomorphology of the Kola Peninsula and Russian Lapland. J. Maps 17 (2), 497–515.
Bradwell, T., Sigurðsson, O., Everest, J., 2013. Recent, very rapid retreat of a temperate glacier in SE Iceland. Boreas 42 (4), 959–973.
Brewer, R., 1976. Fabric and Mineral Analysis of Soils. Krieger, Huntingdon.
Carr, S.J., 1999. The micromorphology of Last Glacial Maximum sediments in the southern North Sea. Catena 35, 123–145.
Carr, S.J., 2001. Micromorphological criteria for discriminating subglacial glacimarine sediments: evidence from a contemporary tidewater glacier, Spitsbergen. Quat. Int. 86, 71–79.
Carr, S.J., 2004. Microscale features and structures. In: Evans, D.J.A., Benn, D.I. (Eds.), A Practical Guide to the Study of Glacial Sediments. Oxford University Press, New York, pp. 115–144.
Carr, S.J., Lee, J.A., 1998. Thin section production of diamicts: problems and solutions. J. Sediment. Res. 68, 217–221.
Chandler, B.M.P., Evans, D.J.A., Roberts, D.H., et al., 2016. Glacial geomorphology of the Skálafellsjökull foreland, Iceland: A case study of 'annual' moraines. J. Maps 12 (5), 904–916.
Chandler, B.M.P., Chandler, S.J.P., Evans, D.J.A., et al., 2020. Sub-annual moraine formation at an active temperate Icelandic glacier. Earth Surf. Process. Landforms 45 (7), 1622–1643.
Charlesworth, J.K., 1928. The Glacial Retreat from Central and Southern Ireland. Quarterly Journal of The Geological Society 84, 293–344.
Chiverrell, R.C., Smedley, R.K., Small, D., Ballantyne, C.K., 2018. Ice margin oscillations during deglaciation of the northern Irish Sea Basin. J. Quat. Sci. 33 (7), 739–762.
Chiverrell, R.C., Thrasher, I.M., Thomas, G.S.P., et al., 2013. Bayesian modelling the retreat of the Irish Sea Ice Stream. J. Quat. Sci. 28 (2), 200–209.
Christoffersen, P., Tulaczyk, S., 2003a. Response of subglacial sediments to basal freeze-on 1. Theory and comparison to observations from beneath the West Antarctic Ice Sheet. J. Geophys. Res. Solid Earth 108 (B4), 2222.
Christoffersen, P., Tulaczyk, S., 2003b. Signature of palaeo-ice-stream stagnation: till consolidation induced by basal freeze-on. Boreas 32 (1), 114–129.
Clark, C.D., 1993. Mega-scale glacial lineations and cross-cutting ice-flow landforms. Earth Surf. Process. Landforms 18 (1), 1–29.
Clark, C.D., Hughes, A.L.C., Greenwood, S.L., et al., 2012. Pattern and timing of retreat of the last British Irish ice sheet. Quat. Sci. Rev. 44 (44), 112–146.
Clark, C.D., Ely, J.C., Greenwood, S.L., et al., 2018. BRITICE Glacial Map, version 2: a map and GIS database of glacial landforms of the last British-Irish Ice Sheet. Boreas 47 (1), 11.
Cline, M.D., Iverson, N.R., Harding, C., 2015. Origin of washboard moraines of the Des Moines Lobe: Spatial analyses with LiDAR data. Geomorphology 246, 570–578.
Cook, S.J., Robinson, Z.P., Fairchild, I.J., et al., 2010. Role of glaciohydraulic supercooling in the formation of stratified facies basal ice: Svínafellsjökull and Skaftafellsjökull, southeast Iceland. Boreas 39 (1), 24–38.
Delaney, C.A., 2002b. Morphology and sedimentology of the Rooskagh esker. Co. Roscommon. Irish Journal of Earth Sciences 19, 12–21.
Delaney, C.A., 2002a. Sedimentology of a glaciofluvial landsystem, Lough Ree area, Central Ireland: implications for ice margin characteristics during Devensian deglaciation. Sediment. Geol. 149, 111–126.
Delaney, C.A., 2001. Esker formation and the nature of deglaciation: the Ballymahon esker, central Ireland. North West Geography, 1(2),22-33. http://www.mangeogsoc.org.uk/publications/north-west-geography/volume-1-2001/.
Delaney, C.A., 2019. Glacial Deposits in the Irish Midlands. INQUA 2019 Field Guide M:GL-5. Irish Quaternary Association, Dublin.
Delaney, C.A., 2022. The development and impact of an ice-contact proglacial lake during the Last Glacial Termination, Palaeolake Riada, central Ireland. J. Quat. Sci. 37 (8), 1422–1441.
Delaney, C.A., McCarron, S., Davis, S., 2018. Irish Ice Sheet dynamics during deglaciation of the central Irish Midlands: Evidence of ice streaming and surging from airborne LiDAR. Geomorphology 306, 235–253.
Dowling, T.P.F., Möller, P., Spagnolo, M., 2016. Rapid subglacial streamlined bedform formation at a calving bay margin. J. Quat. Sci. 31 (8), 879–892.
Dunlop, P., Clark, C.D., 2006. The morphological characteristics of ribbed moraine. Quat. Sci. Rev. 25 (13), 1668–1691.
Dyke, A.S., Evans, D.J.A., 2003. Ice-marginal terrestrial landsystems: northern Laurentide and Innuitian ice sheet margins. In: Evans, D.J.A. (Ed.), Glacial Landsystems. Hodder Arnold, London, pp. 143–165.

Dyke, A.S., Prest, V., 1987. Late Wisconsinan and Holocene History of the Laurentide Ice Sheet. Géogr. Phys. Quaternaire 41 (2), 237–263.
Dyke, A.S., Andrews, J.T., Clark, P.U., et al., 2002. The Laurentide and Innuitian ice sheets during the Last Glacial Maximum. Quat. Sci. Rev. 21, 9–31.
ESRI, 2022. World Imager (Clarity) Overview [Online] Available at: Accessed https://hub.arcgis.com/maps/esri::world-imagery-clarity/about. (Accessed 16 August 2022).
Evans, D.J.A., 2009. Controlled moraines: origins, characteristics and palaeoglaciological implications. Quat. Sci. Rev. 28 (3), 183–208.
Evans, D.J.A., 2010. Controlled moraine development and debris transport pathways in polythermal plateau icefields: examples from Tungnafellsjökull, Iceland. Earth Surf. Process. Landforms 35, 1430–1444.
Evans, D.J.A., 2018. Till. A Glacial Process Sedimentology. Wiley Blackwell, Chichester.
Evans, D.J.A., Hiemstra, J.F., 2005. Till deposition by glacier submarginal, incremental thickening. Earth Surf. Process. 30 (13), 1633–1662.
Evans, D.J.A., Rea, B.R., 1999. Geomorphology and sedimentology of surging glaciers: a land-systems approach. Ann. Glaciol. 28, 75–82.
Evans, D.J.A., Rea, B.R., 2003. Surging glacier landsystem. In: Evans, D.J.A. (Ed.), Glacial Landsystems. Hodder Arnold, London, pp. 259–288.
Evans, D.J.A., Twigg, D.R., 2002. The active temperate glacial landsystem: a model based on Breiðamerkurjökull and Fjallsjökull, Iceland. Quat. Sci. Rev. 21 (20–22), 2143–2177.
Evans, D.J.A., Hiemstra, J.F., O'Cofaigh, C., 2007. An assessment of clast macrofabrics in glacigenic sediments based on A/B plane data. Geogr. Ann. 89A (2), 103–120.
Evans, D.J.A., Strzelecki, M., Milledge, D.G., Orton, C., 2012. Hørbyebreen polythermal glacial landsystem, Svalbard. J. Maps 8 (2), 146–156.
Evans, D.J.A., Young, N.J.P., Ó Cofaigh, C., 2014. Glacial geomorphology of terrestrial-terminating fast flow lobes/ice stream margins in the southwest Laurentide Ice Sheet. Geomorphology 204, 86–113.
Evans, D.J.A., Roberts, D.H., Evans, S.C., 2016a. Multiple subglacial till deposition: a modern exemplar for Quaternary palaeoglaciology. Quat. Sci. Rev. 145, 183–203.
Evans, D.J.A., Storrar, R.D., Rea, B.R., 2016b. Crevasse-squeeze ridge corridors: diagnostic features of late-stage palaeo-ice stream activity. Geomorphology 258, 40–50.
Evans, D.J.A., Roberts, D.H., Hiemstra, J.F., et al., 2018. Submarginal debris transport and till formation in active temperate glacier systems: the southeast Iceland type locality. Quat. Sci. Rev. 195, 72–108.
Evans, D.J.A., Smith, I.R., Gosse, J.C., Galloway, J.M., 2021. Glacial landforms and sediments (landsystem) of the Smoking Hills area, Northwest Territories, Canada: implications for regional Pliocene-Pleistocene Laurentide Ice Sheet dynamics. Quat. Sci. Rev. 262, 106958.
Evans, D.J.A., Ewertowski, M., Roberts, D.H., Tomczyk, A.M., 2022. The historical emergence of a geometric and sinuous ridge network at the Hørbyebreen polythermal glacier snout, Svalbard and its use in the interpretation of ancient glacial landforms. Geomorphology 406, 108213.
Ewertowski, M.W., Tomczyk, A.M., 2020. Reactivation of temporarily stabilized ice-cored moraines in front of polythermal glaciers: Gravitational mass movements as the most important geomorphological agents for the redistribution of sediments (a case study from Ebbabreen and Ragnarbreen, Svalbard. Geomorphology 350, 106952.
Eyles, N., Boyce, J.I., Barendregt, R.W., 1999. Hummocky moraine: sedimentary record of stagnant Laurentide ice sheet lobes resting on soft beds. Sediment. Geol. 123, 163–174.
Farrington, A., Synge, F.M., 1970. The eskers of the Tullamore district. In: Stephens, N., Glasscock, R.E. (Eds.), Irish Geographical Studies in Honour of E. Estyn Evans. Belfast. Queens University, pp. 49–52.
Flink, A.E., Noormets, R., Frasner, O., et al., 2017. Past ice flow in Wahlenbergfjorden and its implications for late Quaternary ice sheet dynamics in northeastern Svalbard. Quat. Sci. Rev. 163, 162–179.
Flint, R.F., 1930. The origin of the Irish "eskers. Geogr. Rev. 20 (4), 615–630.
Florentine, C., Skidmore, M., Speece, M., et al., 2017. Geophysical analysis of transverse ridges and internal structure at Lone Peak Rock Glacier, Big Sky, Montana, USA. J. Glaciol. 60 (221), 453–462.
Fountain, A.G., Schlichting, R.B., Jansson, P., Jacobel, R.W., 2005. Observations of englacial water passages: a fracture-dominated system. Ann. Glaciol. 40, 25–30.
Gallagher, C., Thorp, M., Steenson, P., 1996. Glacier dynamics around Slieve Bloom, Central Ireland. Ir. Geogr. 29 (2), 67–82.
Geological Survey of Ireland, 2017. Quaternary Sediments of Ireland [Online] Available at: http://www.gsi.ie/mapping.htm [Accessed July 2017].
Glasser, N.F., Hambrey, M.J., 2003. Ice-marginal terrestrial landsystems: Svalbard polythermal glaciers. In: Evans, D.J.A. (Ed.), Glacial Landsystems. Hodder Arnold, London, pp. 65–88.
Glasser, N.F., Hambrey, M.J., Etienne, J.L., et al., 2003. The Origin and Significance of Debris-charged Ridges at the Surface of Storglaciären, Northern Sweden. Geografiska Annaler Series A 85 (2), 127–147.
Greenwood, S.L., Clark, C.D., 2009a. Reconstructing the last Irish Ice Sheet 1 : changing flow geometries and ice flow dynamics deciphered from the glacial landform record. Quat. Sci. Rev. 28 (27), 3085–3100.
Greenwood, S.L., Clark, C.D., 2009b. Reconstructing the last Irish Ice Sheet 2: a geomorphologically-driven model of ice sheet growth, retreat and dynamics. Quat. Sci. Rev. 28 (27), 3101–3123.
Guðmundsson, S., Evans, D.J.A., 2022. Geomorphological map of Breiðamerkursandur 2018: the historical evolution of an active temperate glacier foreland. Geografiska Annaler Series A 104 (4), 298–332.
Gulley, J., Benn, D.I., Müller, D., Luckman, A., 2009. A cut-and-closure origin for englacial conduits in uncrevassed regions of polythermal glaciers. J. Glaciol. 55 (189), 66–80.
Gustavson, T.C., Boothroyd, J.C., 1987. A depositional model for outwash, sediment sources, and hydrological characteristics, Malaspina Glacier, Alaska: a modern analog of the southeast margin of the Laurentide ice sheet. Geol. Soc. Am. Bull. 99, 187–200.
Ham, N.R., Attig, J.W., 2001. Minor end moraines of the Wisconsin Valley Lobe, north-central Wisconsin, U.S.A. Boreas 30, 31–41.
Hambrey, M.J., Huddart, D., Bennett, M.R., Glasser, N.F., 1997. Genesis of 'hummocky moraines' by thrusting in glacier ice: evidence from Svalbard and Britain. J. Geol. Soc. 154 (4), 623–632.
Hart, J.K., Clayton, A.I., Martinez, K., Robson, B.A., 2018. Erosional and depositional subglacial streamlining processes at Skálafellsjökull, Iceland: an analogue for a new bedform continuum model. GFF 140 (2), 153–169.
Hicock, S.R., 1990. Genetic till prism. Geology 18 (6), 517–519.
Hiemstra, J.F., 2001. Microscopic analyses of Quaternary glacigenic sediment of Marguerite Bay, Antarctic Peninsula. Arctic Antarct. Alpine Res. 33, 258–265.
Hiemstra, J.F., Rijsdijk, K.F., 2003. Observing artificially induced strain: implications for subglacial deformation. J. Quat. Sci. 18 (5), 373–383.
Hiemstra, J.F., Matthews, J.A., Evans, D.J.A., Owen, G., 2015. Sediment fingerprinting and the mode of formation of singular and composite annual moraine ridges at two glacier margins, Jotunheimen, southern Norway. Holocene 25 (11), 1772–1785.
Hillier, J.K., Benediktsson, Í.Ö., Dowling, T.P.F., Schomacker, A., 2008. Production and preservation of the smallest drumlins. GFF 140 (2), 136–152.
Hoppe, G., 1952. Hummock moraine regions with special reference to the interior of Norbotten. Geogr. Ann. 34, 1–71.
Hughes, A.L.C., Gyllencreutz, R., Lohne, Ø.S., et al., 2016. The last Eurasian ice sheets – a chronological database and time-slice reconstruction, DATED-1. Boreas 45 (1), 1–45.
Irvine-Fynn, T.D.L., Hodson, A.J., Moorman, B.J., et al., 2011. Polythermal glacier hydrology: a review. Rev. Geophys. 49, RG4002.
Jakobsen, P.R., Overgaard, T., 2002. Georadar facies and glaciotectonic structures in ice marginal deposits, northwest Zealand, Denmark. Quat. Sci. Rev. 21 (8–9), 917–927.
Johnson, M.D., Mickelson, D.M., Clayton, L., Attig, J.W., 1995. Composition and genesis of glacial hummocks, western Wisconsin. U.S.A. Boreas 24, 97–116.
Jol, H.M., Bristow, C.S., 2003. An introduction to ground penetrating radar (GPR) in sediments. Geol. Soc., London, Spec. Publ. 211, 1–7.
Jónsson, S.A., Benediktsson, Í.Ö., Ingólfsson, Ó., et al., 2016. Submarginal drumlin formation and late Holocene history of Fláajökull, southeast Iceland. Annals of Glaciology 57, 128–141.
Karušs, J., Lamsters, K., Sobota, I., et al., 2021. Drainage system and thermal structure of a High Arctic polythermal glacier: Waldemarbreen, western Svalbard. J. Glaciol. 68 (269), 591–604.
Kilfeather, A.A., Ó Cofaigh, C., Dowdeswell, J.A., van der Meer, J.J.M., Evans, D.J.A., 2010. Micromorphological characteristics of glacimarine sediments: implications for distinguishing genetic processes of massive diamicts. Geo Mar. Lett. 30, 70–97.
King, E.C., Hindmarsh, R.C.A., Stokes, C.R., 2009. Formation of mega-scale glacial lineations observed beneath a West Antarctic ice stream. Nat. Geosci. 2 (8), 585–588.
Kleman, J., Applegate, P.J., 2014. Durations and propagation patterns of ice sheet instability events. Quat. Sci. Rev. 92, 32–39.
Knight, J., McCarron, S.G., McCabe, A.M., 1999. Landform modification by palaeo-ice streams in east-central Ireland. Ann. Glaciol. 28, 161–167.
Kokalj, Ž., Somrak, M., 2019. Why not a single image? Combining visualizations to facilitate fieldwork and on-screen mapping. Rem. Sens. 11 (7), 747.
Krüger, J., 1993. Moraine-ridge formation along a stationary ice front in Iceland. Boreas 22 (2), 101–109.
Krüger, J., 1995. Origin, chronology and climatological significance of annual-moraine ridges at Myrdalsjökull, Iceland. Holocene 5 (4), 420–427.
Krüger, J., 1996. Moraine ridges formed from subglacial frozen-on sediment slabs and their differentiation from push moraines. Boreas 25 (1), 57–64.
Krüger, J., Kjaer, K.H., Schomacker, A., 2010a. 7 Dead-Ice Environments: A Landsystems Model for a Debris-Charged, Stagnant Lowland Glacier Margin. Kötlujökull. Developments in Quaternary Sciences 13, 105–126.
Krüger, J., Schomacker, A., Benediktsson, Í.Ö., 2010b. Ice-marginal environments: geomorphic and structural genesis of marginal moraines at Mýrdalsjökull. Dev. Quat. Sci. 13, 79–104.
Lachniet, M.S., Larson, G.J., Strasser, J.C., et al., 1999. Microstructures of glacigenic sediment-flow deposits, Matanuska Glacier, Alaska. In: Mickelson, D.M., Attig, J.W. (Eds.), Glacial Processes Past and Present, vol. 337. Geological Society of America Special Paper, pp. 45–57.
Lachniet, M.S., Larson, G.J., Lawson, D.E., Evenson, E.B., Alley, R.B., 2001. Microstructures of sediment flow deposits and subglacial sediments: a comparison. Boreas 30, 254–262.
Larsen, G.J., Menzies, J., Lawson, D.E., et al., 2016. Macro- and micro-sedimentology of a modern melt-out till - Matanuska Glacier, Alaska, USA. Boreas 45, 235–251.
Lawson, D.E., 1982. Mobilization, Movement and Deposition of Active Subaerial Sediment Flows, Matanuska Glacier, Alaska. J. Geol. 90 (3), 279–300.
Lawson, D.E., Trasser, J.C., Evenson, E.B., et al., 1998. Glaciohydraulic supercooling: a freeze-on mechanism to create stratified, debris-rich basal ice. I. Field evidence. J. Glaciol. 44 (148), 547–562.

Lee, J., Kemp, R., 1993. Thin Sections of Unconsolidated Sediments and Soils: A Recipe. Department of Geography, Royal Holloway University of London, London (unpublished).
Leigh, S., Hartley, A.J., 1992. Mega-debris flow deposits from the Oligo-Miocene Pindos foreland basin, western mainland Greece: implications for transport mechanisms in ancient deep marine basins. Sedimentology 39 (6), 1003–1012.
Lewington, E.L.M., Livingstone, S.J., Clark, C.D., Sole, A.J., Storrar, R.D., 2020. A model for interaction between conduits and surrounding hydraulically connected distributed drainage based on geomorphological evidence from Keewatin, Canada. Cryosphere 14, 2949–2976.
Linch, L.D., Dowdeswell, J.A., 2016. Micromorphology of diamicton affected by iceberg-keel scouring, Scoresby Sund, East Greenland. Quat. Sci. Rev. 152, 169–196.
Linch, L.D., van der Meer, J.J.M., 2014. Micromorphology of ice keel scour in pebbly sandy mud and fine-grained sands: Scarborough Bluffs, Ontario, Canada. Sedimentology 62, 110–129.
Linch, L.D., van der Meer, J.J.M., Menzies, J., 2012. Micromorphology of iceberg scour in clays: Glacial Lake Agassiz, Manitoba, Canada. Quat. Sci. Rev. 55 (8), 125–144.
Lindén, M., Möller, P., 2005. Marginal formation of De Geer moraines and their implications to the dynamics of grounding-line recession. J. Quat. Sci. 20, 113–133.
Lindén, M., Möller, P., Adrielsson, L., 2008. Ribbed moraine formed by subglacial folding, thrust stacking and lee-side cavity infill. Boreas 37 (1), 102–131.
Lowe, D.R., 1976. Subaqueous liquefied and fluidized sediment flows and their deposits. Sedimentology 23 (3), 1976.
Lowe, D.R., 1979. In: Sediment Gravity Flows: Their Classification and Some Problems of Application to Natural Flows and Deposits, vol. 27. S.E.P.M. Spec. Pub., pp. 75–82
Lowe, D.R., 1982. Sediment gravity flows II: depositional models with special reference to the deposits of high-density turbidity currents. J. Sediment. Petrol. 52, 279–297.
Lukas, S., 2005. A test of the englacial thrusting hypothesis of 'hummocky' moraine formaton: case studies from the northwest Highlands, Scotland. Boreas 34 (3), 287–307.
Lukas, S., 2012. Processes of annual moraine formation at a temperate alpine valley glacier: insights into glacier dynamics and climatic controls. Boreas 41 (3), 463–480.
Lukas, S., Nicholson, L.I., Ross, F.H., Humlum, O., 2005. Formation, meltout processes and landscape alteration of High-Arctic ice-cored moraines – examples from Nordenskiold Land, central Spitsbergen. Polar Geogr. 29 (3), 157–187.
Mahaney, W.C., Dirszowsky, R.W., Milner, M.W., et al., 2004. Quartz microtextures and microstructures owing to deformation of glaciolacustrine sediments in the northern Venezuelan Andes. J. Quat. Sci. 19, 23–33.
Margold, M., Stokes, C.R., Clark, C.D., 2015. Ice streams in the Laurentide Ice Sheet : identification, characteristics and comparison to modern ice sheets. Earth Sci. Rev. 143 (143), 117–146.
Matthews, J.A., McCarroll, D., Shakesby, R.A., 1995. Contemporary terminal-moraine ridge formation at a temperate glacier: Styggedalsbreen, Jotunheimen, southern Norway. Boreas 24 (2), 129–139.
McCabe, A.M., 2008. Glacial Geology and Geomorphology - the Landscapes of Ireland. Dunedin Academic Press, Edinburgh.
McCabe, A.M., Clark, P.U., Clark, J., Dunlop, P., 2007. Radiocarbon constraints on readvances of the British–Irish Ice Sheet in the northern Irish Sea Basin during the last deglaciation. Quat. Sci. Rev. 26 (9–10), 1204–1211.
McDonald, B.C., Shilts, W.W., 1975. Interpretation of faults in glaciofluvial sediments. In: Jopling, A.V., McDonald, B.C. (Eds.), Glaciofluvial and Glaciolacustrine Sedimentation, vol. 23. SEPM Special Publication No., pp. 123–132, 1975.
Menzies, J., 1998. Microstructures within subglacial diamictons. In: Relief and Deposits of Present-Day and Pleistocene Glaciations of the Northern Hemisphere - Selected Problems. Adam Mickiewicz University Press, Poznan, pp. 153–166.
Menzies, J., 2000. Micromorphological analyses of microfabrics and microstructures indicative of deformation processes in glacial sediments. In: Maltman, A.J., Hubbard, A.J., Hambrey, M.J. (Eds.), Deformation of Glacial Materials, vol. 176. Geological Society Special Publication, London, pp. 245–257.
Menzies, J., 2012. Strain pathways, till internal architecture and microstructures - perspectives on a general kinematic model - a 'blueprint' for till development. Quat. Sci. Rev. 50, 105–114.
Möller, P., 2006. Rogen moraine: an example of glacial reshaping of pre-existing landforms. Quat. Sci. Rev. 25 (3–4), 362–389.
Möller, P., 2010. Melt-out till and ribbed moraine formation, a case study from south Sweden. Sediment. Geol. 232 (3–4), 161–180.
Möller, P., Dowling, P.F., 2015. The importance of thermal boundary transitions on glacial geomorphology; mapping of ribbed/hummocky moraine and streamlined terrain from LiDAR, over Småland, South Sweden. GFF 137 (4), 252–283.
Monz, M.E., Hudleston, P., Cook, S.J., et al., 2021. Thrust faulting in glaciers? Re-examination of debris bands near the margin of Storglaciären, Sweden. Boreas 51 (1), 78–99.
Mulder, T., Alexander, J., 2001. The physical character of subaqueous sedimentary density flows and their deposits. Sedimentology 48, 269–299.
Narloch, W., Phillips, E.R., Piotrowski, J.A., Cwiek, M., 2020. Patterns of deformation within a subglacial shear zone: implications for palaeo-ice stream bed evolution. Sediment. Geol. 397, 105569.
Neal, A., Pontee, N.I., Pye, K., Richards, J., 2002. Internal structure of mixed-sand-and-gravel beach deposits revealed using ground-penetrating radar. Sedimentology 49, 789–804.
Ó Cofaigh, C., Stokes, C.R., Lian, O.B., et al., 2013. Formation of mega-scale glacial lineations on the Dubawnt Lake Ice Stream bed: 2. Sedimentology and stratigraphy. Quat. Sci. Rev. 77, 210–227.
Ojala, A.E.K., 2016. Appearance of De Geer moraines in southern and western Finland — Implications for reconstructing glacier retreat dynamics. Geomorphology 255, 16–25.
Ojala, A.E.K., Putkinen, N., Palmu, J.P., Nenonen, K., 2015. Characterization of De Geer moraines in Finland based on LiDAR DEM mapping. GFF 137 (4), 304–318.
Ojala, A.E.K., Peterson, G., Mäkinen, J., et al., 2019. Ice sheet scale distribution of unique triangular-shaped hummocks (murtoos) – a subglacial landform produced during rapid retreat of the Scandinavian Ice Sheet. Ann. Glaciol. 60, 115–126.
Palmer, A., Lee, J., Kemp, R., Carr, S., 2008. Revised Laboratory Procedures for the Preparation of Thin Sections from Unconsolidated Sediments. Centre for Micromorphology, University of London, London (unpublished).
Patterson, C.J., 1997. Southern Laurentide ice lobes were created by ice streams: Des Moines Lobe in Minnesota. U.S.A. Sedimentary Geol. 111, 249–261.
Pellicer, X.M., Warren, W.P., Gibson, P., Linares, R., 2012. Construction of an evolutionary deglaciation model for the Irish midlands based on the integration of morphostratigraphic and geophysical data analyses. J. Quat. Sci. 27 (8), 807–818.
Peterson, G., Johnson, M.D., 2017. Hummock corridors in the south-central sector of the Fennoscandian ice sheet, morphometry and pattern. Earth Surf. Process. Landforms 43, 919–929.
Peterson, G., Johnson, M.D., Smith, C.A., 2017. Glacial geomorphology of the south Swedish uplands – focus on the spatial distribution of hummock tracts. J. Maps 13 (2), 534–544.
Phillips, E.R., 2006. Micromorphology of a debris flow deposit: evidence of basal shearing, hydrofracturing, liquefaction and rotational deformation during emplacement. Quat. Sci. Rev. 25, 720–738.
Phillips, E.R., Auton, C., 2000. Micromorphological evidence for polyphase deformation of glaciolacustrine sediments from Strathspey, Scotland. Geol. Soc. London Spec. Publ. 176 (1), 279–292.
Phillips, E.R., van der Meer, J.J.M., Ferguson, A., 2011. A new 'microstructural mapping' methodology for the identification, analysis and interpretation of polyphase deformation within subglacial sediments. Quat. Sci. Rev. 30 (19–20), 2570–2596.
Phillips, E., Everest, J., Reeves, H., 2013. Micromorphological evidence for subglacial multiphase sedimentation and deformation during overpressurized fluid flow associated with hydrofracturing. Boreas 42, 395–427.
Phillips, E.R., Evans, D.J.A., van der Meer, J.J.M., Lee, J.R., 2018. Microscale evidence of liquefaction and its potential triggers during soft-bed deformation within subglacial traction tills. Quat. Sci. Rev. 181, 123–143.
Powers, M.C., 1953. A New Roundness Scale for Sedimentary Particles. J. Sediment. Res. 23 (2), 117–119.
Price, R.J., 1969. Moraines, sandar, kames and eskers near Breiðamerkurjökull, Iceland. Trans. Inst. Br. Geogr. 46, 17–43.
Putniņš, A., Henriksen, M., 2017. Reconstructing the flow pattern evolution in inner region of the Fennoscandian Ice Sheet by glacial landforms from Gausdal Vestfjell area, south-central Norway. Quat. Sci. Rev. 163, 56–71.
Reinardy, B.T.I., Lukas, S., 2009. The sedimentary signature of ice-contact sedimentation and deformation at macro- and micro-scale: a case study from NW Scotland. Sediment. Geol. 221, 87–98.
Reinardy, B.T.I., Leighton, I., Marx, P.J., 2013. Glacier thermal regime linked to processes of annual moraine formation at Midtdalsbreen, southern Norway. Boreas 42, 896–911.
Roberts, M.J., Russell, A.J., Tweed, F.S., Knudsen, Ó., 2000. Ice fracturing during jökulhlaups: implications for englacial floodwater routing and outlet development. Earth Surf. Process. Landforms 25, 1429–1446.
Russell, A.J., Roberts, M.R., Fay, H., et al., 2006. Icelandic jökulhlaup impacts: implications for ice-sheet hydrology, sediment transfer and geomorphology. Geomorphology 75, 33–64.
Sadura, S., Martini, I.P., Endres, A.L., Wolf, K., 2006. Morphology and GPR stratigraphy of a frontal part of an end moraine of the Laurentide Ice Sheet: Paris moraine near Guelph, ON, Canada. Geomorphology 75 (1), 212–225.
Schlegel, R., Murray, T., Smith, A.M., et al., 2022. Radar Derived Subglacial Properties and Landforms Beneath Rutford Ice Stream, West Antarctica. J. Geophys. Res.: Earth Surf. 127 (1), e2021JF006349.
Sevastopulo, G.D., Wyse-Jackson, P.N., 2009. Carboniferous: Mississippian (Tournaisian and Viséan). In: Holland, C., Sanders, I. (Eds.), The Geology of Ireland. Dunedin Academic Press, Edinburgh, pp. 215–268.
Sharp, M., 1985. Crevasse-Fill" Ridges—A Landform Type Characteristic of Surging Glaciers? Geogr. Ann. Phys. Geogr. 67 (4), 213–220.
Shreve, R.L., 1972. Movement of water in glaciers. J. Glaciol. 11 (62), 205–214.
Skidmore, M.L., Sharp, M.J., 1999. Drainage system behaviour of a High-Arctic polythermal glacier. Ann. Glaciol. 28, 209–215.
Sletten, K., Lyså, A., Lønne, I., 2001. Formation and disintegration of a high-arctic ice-cored moraine. Boreas 30, 272–284.
Smith, A.M., Murray, T., 2009. Bedform topography and basal conditions beneath a fast-flowing West Antarctic ice stream. Quat. Sci. Rev. 28 (7–8), 584–596.
Smith, A.M., Murray, T., Nicholls, K.W., et al., 2007. Rapid erosion, drumlin formation, and changing hydrology beneath an Antarctic ice stream. Geology 35 (2), 127–130.
Sollas, W.J., 1896. A Map to Show the Distribution of Eskers in Ireland, vol. 5. Royal Dublin Society Scientific Transactions, pp. 785–822.

Speddings, N., Evans, D.J.A., 2002. Sediments and landforms at Kvıarjokull, south-east Iceland: a reappraisal of the glaciated valley landsystem. Sediment. Geol. 149 (1–3), 21–42.
Stokes, C.R., 2018. Geomorphology under ice streams: Moving from form to process. Earth Surf. Process. Landforms 43 (1), 85–123.
Stokes, C.R., Clark, C.D., 2002. Are long subglacial bedforms indicative of fast ice flow. Boreas 31 (3), 239–249.
Stokes, C.R., Clark, C.D., 2003. The Dubawnt Lake palaeo-ice stream: evidence for dynamic ice sheet behaviour on the Canadian Shield and insights regarding the controls on ice-stream location and vigour. Boreas 32 (1), 263–279.
Stokes, C.R., Lian, O.B., Tulaczyk, S., Clark, C.D., 2008. Superimposition of ribbed moraines on a palaeo-ice-stream bed : implications for ice stream dynamics and shutdown. Earth Surf. Process. Landforms 33 (4), 593–609.
Storrar, R.D., Stokes, C.R., Evans, D.J.A., 2014. Morphometry and pattern of a large sample (>20,000) of Canadian eskers and implications for subglacial drainage beneath ice sheets. Quat. Sci. Rev. 105, 1–25.
Storrar, R.D., Evans, D.J.A., Stokes, C.R., Ewertowski, M., 2015. Controls on the location, morphology and evolution of complex esker systems at decadal timescales, Breiɗamerkurjökull, southeast Iceland. Earth Surf. Process. Landforms 40 (11), 1421–1438.
Storrar, R.D., Ewertowski, M., Tomczyk, A.M., et al., 2020. Equifinality and preservation potential of complex eskers. Boreas 49 (1), 211–231.
Sundal, A.V., Shepherd, A., Nienow, P., et al., 2011. Melt-induced speed-up of Greenland ice sheet offset by efficient subglacial drainage. Nature 469, 521–524.
Swift, D.A., Evans, D.J.A., Fallick, A.E., 2006. Transverse englacial debris-rich ice bands at Kvíárjökull, southeast Iceland. Quat. Sci. Rev. 25 (13), 1708–1718.
Swift, D.A., Cook, S.J., Graham, D.J., et al., 2018. Terminal zone glacial sediment transfer at a temperate overdeepened glacier system. Quat. Sci. Rev. 180, 111–131.
Synge, F.M., 1979. Quaternary glaciation in Ireland. Quat. Newsl. 28, 1–18.
Talling, P.J., Masson, D.G., Sumner, E.J., Malgesini, G., 2012. Subaqueous sediment density flows: depositional processes and deposit types. Sedimentology 59, 1937–2003.
Tedstone, A.J., Nienow, P.W., Gourmelen, N., et al., 2015. Decadal slowdown of a land-terminating sector of the Greenland Ice sheet despite warming. Nature 526, 692–695.
Tonkin, T.N., Midgley, N.G., Cook, S.J., Graham, D.J., 2016. Ice-cored moraine degradation mapped and quantified using an unmanned aerial vehicle: A case study from a polythermal glacier in Svalbard. Geomorphology 258, 1–10.
Tonkin, T.N., Midgley, N.G., Graham, D.J., Labadz, J.C., 2017. Internal structure and significance of ice-marginal moraine in the Kebnekaise Mountains, northern Sweden. Boreas 46 (2), 199–211.
van der Meer, J.J.M., 1993. Microscopic evidence of subglacial deformation. Quat. Sci. Rev. 12, 553–587.
van der Meer, J.J.M., 1995. Micromorphology. In: Menzies, J. (Ed.), Past Glacial Environments: Sediments, Forms and Techniques. Butterworth-Heinemann, Oxford, pp. 335–355.
van der Meer, J.J.M., Menzies, J., 2011. The micromorphology of unconsolidated sediments. Sediment. Geol. 238, 213–232.
van der Meer, J.J.M., Carr, S.J., Kjaer, K.H., 2010. 10 Mýrdalsjökull's Forefields Under the Microscope. The Micromorphology of Meltout and Subglacial Tills. Dev. Quat. Sci. 13, 159–180.
Vérité, J., Ravier, É., Bourgeois, O., et al., 2021. Formation of ribbed bedforms below shear margins and lobes of palaeo-ice streams. Cryosphere 15, 2889–2916.
Vérité, J., Ravier, É., Bourgeois, O., et al., 2022. Formation of murtoos by repeated flooding of ribbed bedforms along subglacial meltwater corridors. Geomorphology 408, 108248.
Warren, W.P., 1992. Drumlin orientation and the pattern of glaciation in Ireland. Severiges Geologiska Undersökning Ser. Ca 81, 359–366.
Zakšek, K., Oštir, K., Kokalj, Ž., 2011. Sky-view factor as a relief visualization technique. Rem. Sens. 3, 398–415.
Zilliacus, H., 1989. Genesis of De Geer moraines in Finland. Sediment. Geol. 62 (2–4), 309–317.